Ore Geology Reviews 88 (2017) 400–415

Contents lists available at ScienceDirect

Ore Geology Reviews

journal homepage: www.elsevier.com/locate/oregeo

Ore petrology, hydrothermal alteration, fluid inclusions, and sulfur stable isotopes of the Milin Kamak intermediate sulfidation epithermal Au-Ag deposit in Western Srednogorie, Bulgaria

Ralica Sabeva [a,*], Vassilka Mladenova [a], Aberra Mogessie [b]

[a] Sofia University, FGG, 1504 Sofia, Bulgaria
[b] Institute of Earth Sciences, University of Graz, Univ. Pl. 2, A-8010 Graz, Austria

ARTICLE INFO

Article history:
Received 12 August 2016
Received in revised form 10 May 2017
Accepted 14 May 2017
Available online 22 May 2017

Keywords:
Milin Kamak
Bulgaria
Gold
Hydrothermal alteration
Fluid inclusions
Sulfur stable isotopes

ABSTRACT

The Milin Kamak gold-silver deposit is located in Western Srednogorie zone, 50 km west of Sofia, Bulgaria. This zone belongs to the Late Cretaceous Apuseni-Banat-Timok-Srednogorie magmatic and metallogenic belt. The deposit is hosted by altered trachybasalt to andesitic trachybasalt volcanic and volcanoclastic rocks with Upper Cretaceous age, which are considered to be products of the Breznik paleovolcano. Milin Kamak is the first gold-silver intermediate sulfidation type epithermal deposit recognized in Srednogorie zone in Bulgaria. It consists of eight ore zones with lengths ranging from 400 to 1000 m, widths from several cm to 3–4 m, rarely to 10–15 m, an average of 80–90 m depth (a maximum of 200 m) and dip steeply to the south. The average content of gold is 5.04 g/t and silver – 13.01 g/t. The styles of alteration are propylitic, sericite, argillic, and advanced argillic. Ore mineralization consists of three stages. Quartz-pyrite stage I is dominated by quartz, euhedral to subhedral pyrite, trace pyrrhotite and hematite in the upper levels of the deposit. Quartz-polymetallic stage II is represented by major anhedral pyrite, galena, Fe-poor sphalerite; minor chalcopyrite, tennantite, bournonite, tellurides and electrum; and trace pyrrhotite, arsenopyrite, marcasite. Gangue minerals are quartz and carbonates. The carbonate-gold stage III is defined by deposition of carbonate minerals and barite with native gold and stibnite.

Fluid inclusions in quartz are liquid H_2O-rich with homogenization temperature (T_h) ranging from 238 to 345 °C as the majority of the measurements are in the range 238–273 °C. Ice-melting temperatures (T_m) range from −2.2 to −4.1 °C, salinity – from 3.7 to 6.6 wt.% NaCl equiv. These measurements imply an epithermal environment and low- to moderate salinity of the ore-forming fluids.

$\delta^{34}S$ values of pyrite range from −0.49 to +2.44‰. The average calculated $\delta^{34}S$ values are 1.35‰. The total range of $\delta^{34}S$ values for pyrite are close to zero suggesting a magmatic source for the sulfur.

1. Introduction

Since Lindgren (1933), over the past several decades there have been numerous studies of different epithermal systems, especially the two end members – low and high sulfidation type deposits (Heald et al., 1987; Evans, 1993; Arribas, 1995; White and Hedenquist, 1995; Cooke and Simmons, 2000; Einaudi et al., 2003; Pirajno, 2009). After the works of Hedenquist et al. (2000), Einaudi et al. (2003), Sillitoe and Hedenquist (2003) the number of publications showing worldwide examples of intermediate sulfidation type deposits have increased.

Previous studies at the Milin Kamak area dealt with preliminary data of the mineral composition, alteration and some genetic aspects (Crummy et al., 2001; Stoykov et al., 2007). The aim of this investigation is to document the ore minerals, their textures, alteration assemblages, fluid inclusions in quartz, and sulfur isotope in pyrite. These new data will help to constrain the ore-forming environment and the significance of the ore potential of the prospect.

2. Geological settings

2.1. Regional geology

The Milin Kamak deposit is situated in the Western Srednogorie zone in Bulgaria which in regional aspect belongs to the Late

* Corresponding author.
E-mail address: rsabeva@gea.uni-sofia.bg (R. Sabeva).

http://dx.doi.org/10.1016/j.oregeorev.2017.05.013
0169-1368/

Cretaceous Apuseni-Banat-Timok-Srednogorie (ABTS) magmatic and metallogenic belt (Popov et al., 2002), known also as the Banatitic magmatic and metallogenic belt (Berza et al., 1998). It is one of the main structures of the Alpine-Balkan-Carpathian-Dinaride geodynamic province (Ciobanu et al., 2002; Heinrich and Neubauer, 2002; Neubauer and Heinrich, 2003) (Fig. 1). The ABTS belt was formed as a result of the subduction of the Tethys Ocean beneath the European continental margin during the Late Cretaceous phase of the Alpine-Himalayan orogeny. It can be traced from the Apuseni Mountains and Banat region in Romania, through the Timok area in Serbia to the Srednogorie zone in Bulgaria. It extends for about 1000 km with a width of 30–120 km. Late Cretaceous magmatic products are extrusive and intrusive rocks exposed as large volcano-plutonic complexes. The compositional trends vary from tholeiitic to high-K-alkaline, and shoshonitic, with dominant calc-alkaline and high-K calc-alkaline types (Popov et al., 2002; Ciobanu et al., 2002; Kamenov et al., 2003; von Quadt et al., 2005; Popov et al., 2012).

The Srednogorie part of the ABTS belt in Bulgaria is developed during the Mesozoic as an island arc system (Janković, 1977; Heinrich and Neubauer, 2002; Dabovski et al., 2009; Popov et al., 2012) (Fig. 1). It is an 80–100 km wide and east–west oriented zone, located between the Balkan Zone in the north, and the Rhodopes and the Sakar-Strandzha zone in the south (Bonchev, 1988; Ivanov, 1998). Western Srednogorie consists of volcanoclastic, volcanic and intrusive rocks and sediments with Upper Cretaceous age. Magmatic rocks result from the activity of seven volcanic complexes which formed during Coniacian-Campanian (Stanisheva-Vassileva, 1980; Dabovski et al., 1991).

The ABTS belt is an economically important province which hosts Cu- and Au-rich porphyry and high, intermediate and low sulfidation type deposits (Berza et al., 1998; Ciobanu et al., 2002; Heinrich and Neubauer, 2002; Popov et al., 2002; von Quadt et al., 2005). A large number of ore deposits have formed in the Srednogorie, but the world-class deposits are concentrated in the Panagyurishte region in the central parts of the zone. The porphyry-copper deposits are Elatsite, Medet, Assarel, Tsar Asen and Vlaykov Vruh. The Cu-Au epithermal high sulfidation type deposits are Elshitsa, Radka, Krassen and Chelopech (Bogdanov, 1987; Popov et al., 2000; Strashimirov et al., 2002; Moritz et al., 2004; von Quadt et al., 2005; Bogdanov and Mišković, 2014).

The Western Srednogorie zone, which is not well prospected, hosts mainly gold and copper occurrences – such as Zlatousha (Ferdov and Kunov, 2002), Klisoura (Kunov et al., 2000) and the Gurgulyatski Kamak area (Nakov et al., 2010; Nakov et al., 2016).

2.2. Local geology and characteristics of the Milin Kamak deposit

Milin Kamak deposit is located 50 km west of Sofia and 2 km south of the town of Breznik between the Bor-Majdanpek gold-copper ore district in Serbia to the north-west and the Panagyurishte district to the east (Fig. 1). It is situated in Western

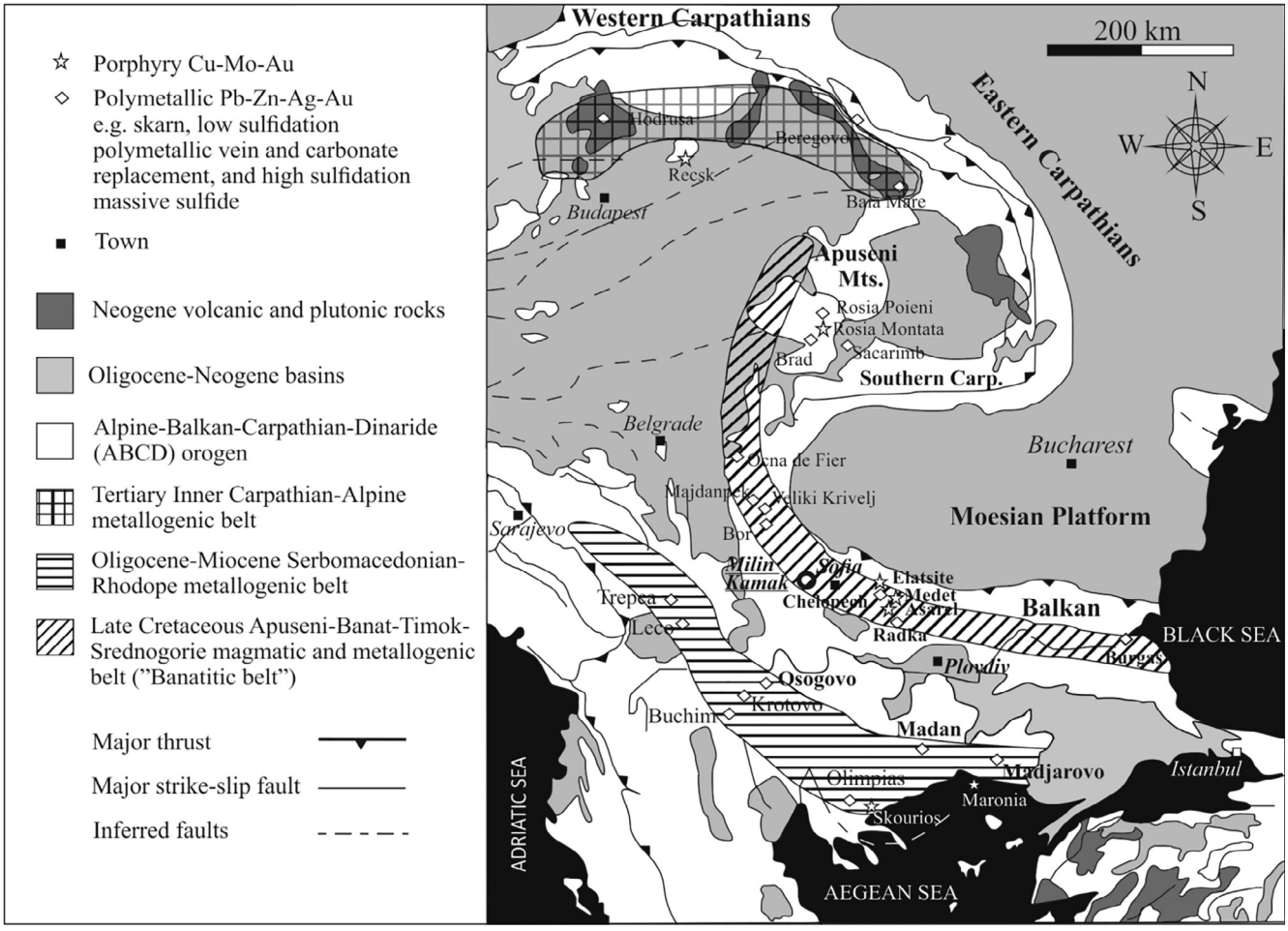

Fig. 1. Simplified geological and tectonic map showing the distribution of the principal ore deposits zones in the Balkan-Carpathian-Dinaride region. Three mineralized belts are developed with calc-alkaline magmatism of Late-Cretaceous to Miocene age (after Heinrich and Neubauer (2002) modified by Chambefort (2005)). The Milin Kamak deposit is situated in Cretaceous Apuseni-Banat-Timok-Srednogorie magmatic and metallogenic belt.

Srednogorie zone in the Bardoto hill, formed by the stratocone of the Breznik paleovolcano.

Products of the Breznik paleovolcano belong to the Upper volcanogenic-sedimentary unit (Nachev et al., 1981; Bairaktarov, 1989; Dabovski et al., 2009) (Fig. 2A). The rocks are volcaniclastic products and lava flows, dykes are rare. In the northern part subvolcanic bodies form a chain with subequatorial orientation and elliptical outlines having a diameter of about 10 m with concentric and radial joints. The subvolcanic bodies are a group of fracture controlled magmatic vents. The rocks are mainly trachybasalts and shoshonites referred to the high potassium calc-alkaline to shoshonitic series (Dabovski et al., 2009; Velev et al., 2012).

The Milin Kamak deposit is hosted by altered trachybasalt to andesitic trachybasalt volcanic and volcanoclastic rocks (Bairaktarov, 1989; Dabovski et al., 2009; Velev et al., 2012). A part of the sequence is overlain by Paleogene and Neogene sediments. In the south-west, a Permian to Jurassic sequence of continental to marine sediments, represented by sandstones, clay and limestone, is observed (Belev, 1967) (Fig. 2B). Small diorite porphyry stocks and porphyrytic basalt dykes with a geophysical IP anomaly established in the Milin Kamak area, suggest a diorite intrusive at depth covering about 10 km^2 (Crummy et al., 2001).

The deposit is situated south-west of the Krasava syncline. Paleogene sediments build up the axial parts, the limbs of the syncline are composed of Upper Cretaceous volcanic and volcanogenic-sedimentary rocks. The later overly Lower Cretaceous and Triassic to Jurassic terrigenous-carbonate sediments.

Major NW-striking faults parallel to paleo-subduction direction of Western Srednogorie zone, and secondary NE-striking, crosscutting normal faults and shear zones are mapped in the area. The secondary E-W-striking faults host the ore mineralization.

The Milin Kamak deposit comprises of eight ore zones, represented by epithermal veins (Fig. 3A). The ore zones have a varying length from 400 to 1000 m, from several cm to 3–4 m wide, rarely to 10–15 m, an average 80–90 m depth (a maximum of 200 m) and dip steeply to the south (Fig. 3B). The main ore zone, marked as No. 1 zone reaches 200 m depth. It presently represents the economic part of the deposit. The No. 4 and No. 8 zones are located in the northern part of the deposit but are not well explored. The highest Cu contents are established in No. 8 zone. Zone No. 2, 3, 5 and 6 are in close spatial relationship with the main zone and have similar morphological and textural characteristics.

The area was explored by Trace Resources Ltd. between 2004 and 2012 with 100 trenches and 121 drill holes. Eight ore zones

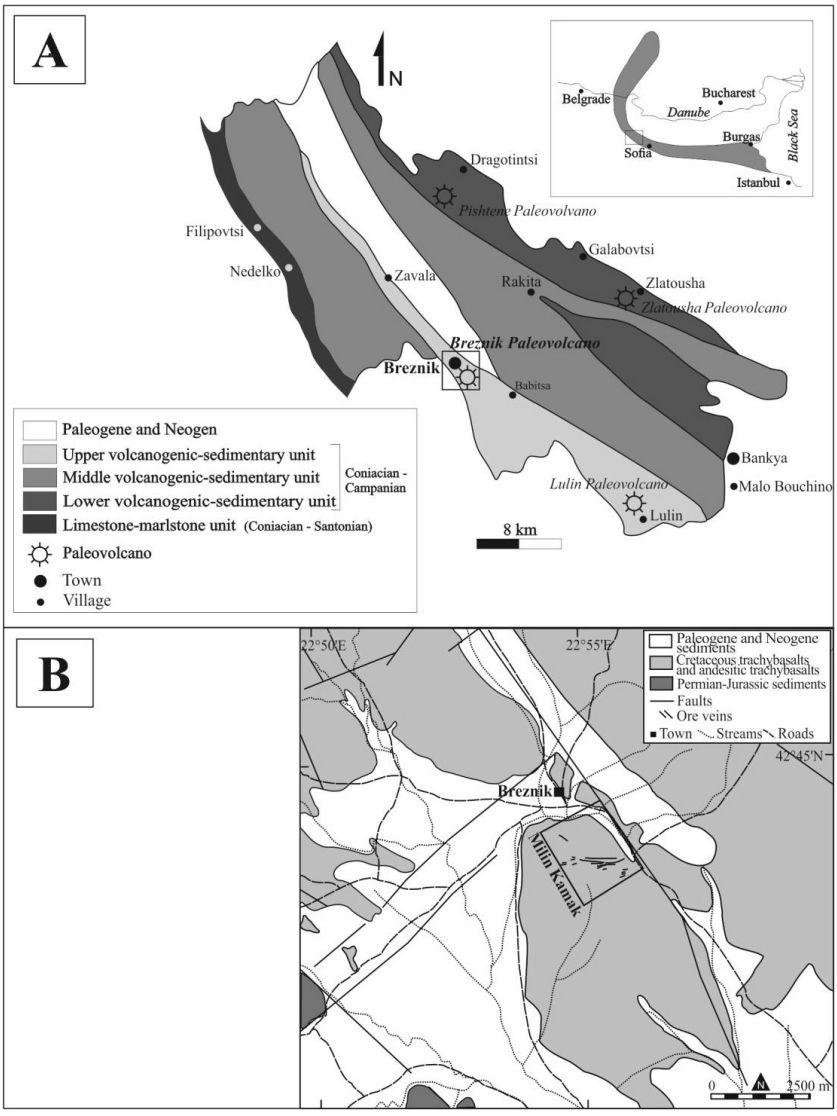

Fig. 2. (A) Simplified geological map of Western Srednogorie zone in Bulgaria with the main paleovolcanic centres (after Dabovski et al. (2009) modified by Velev et al. (2012)). (B) Simplified geological map of Milin Kamak area.

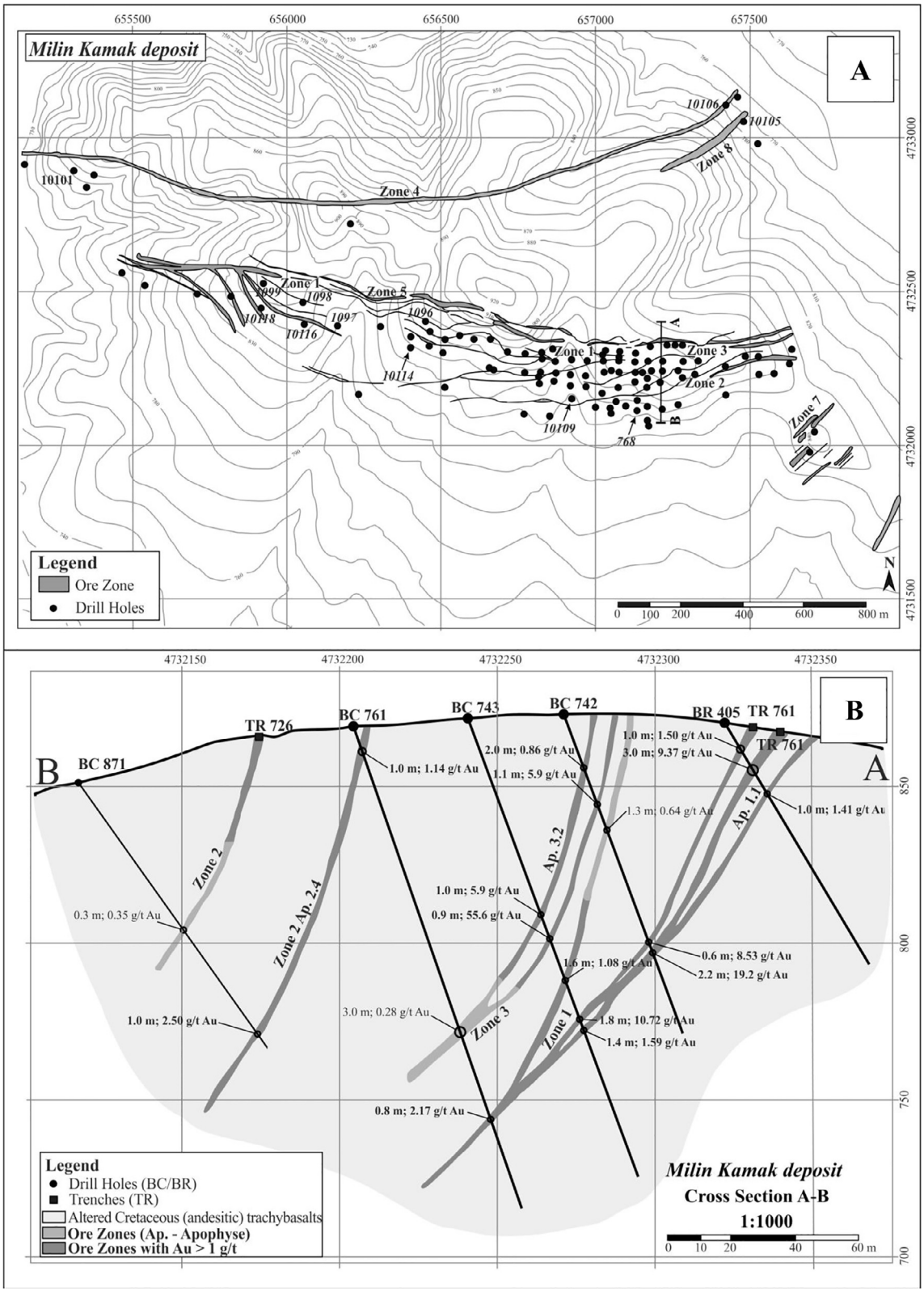

Fig. 3. (A) Location of the ore zones and drill holes in the Milin Kamak area. The profile line A-B is represented by cross section at Fig. 3B. The sampled drill holes are indicated with numbers. (B) Cross section A-B transecting the main No. 1, No. 3 and 2 ore zones. The veins dip steeply to south.

of almost identical mineral composition were established. On the basis of these results, at a cut-off grade of 2 g/t and a total volume 2.4 Mt with an average content of gold 5.91 g/t and of silver 26.78 g/t, the probable reserves and resources are 13.132 tonnes of gold and 59.537 tonnes of silver (Trace Resources Ltd.).

3. Sampling and analytical techniques

The samples from hydrothermal altered rocks and epithermal veins are collected from 12 drill holes intersecting 5 mineralized zones (Fig. 3A).

Polished sections and polished thin sections were prepared to determine the paragenetic relationships of the ore minerals and to characterize the hydrothermal alteration assemblages. Ore samples were observed by optical microscope Opton Universal Pol-U.

X-ray powder diffraction (XRD) analyses were performed on a TUR M62 diffractometer using filtered Co-Kα radiation in the 2θ range 4–80°, step size 1.5° at Sofia University "St. Kliment Ohridski", Sofia, Bulgaria.

Electron microprobe analyses (EMPA) and back-scattered electron imaging were done on carbon-coated polished sections with a SEM JEOL JSM 6310 equipped with an Oxford Link ISIS EDX system and a Microspec WDX system at the Institute of Earth Sciences, University of Graz, Austria. Analytical conditions were: 20 kV accelerating voltage, 6 nA probe current, and 100 s counting time for EDX spectra. Standards used were $CuFeS_2$ (S, Fe, Cu), metallic Mn, ZnS (Zn), Pd_3As (As), CuSe (Se), metallic Ag, metallic Cd, NiSb (Sb), PbTe (Te, Pb), and Bi_2Te_3 (Bi). The detection limits for the EDX are 0.1 wt.% for Ag, Au, Cu, Co, Fe, Zn; 0.2 wt.% for Sb, Te, Cd; 0.5 wt.% for As; 0.9 wt.% for Bi; 1.5 wt.% for Pb. The gangue minerals and some ore minerals were also examined with microprobe analyses with JEOL Superprobe 733 equipped with an ORTEC EDX system and a Tracor Northern TN-2000 system, Geological Institute, Bulgarian Academy of Sciences, Sofia, Bulgaria. Analytical conditions were: 15 and 25 kV accelerating voltage, 0.5 nA probe current.. Standards used were $CuFeS_2$ (S, Fe, Cu), FeS_2 (Fe, S), CdS (Cd), ZnS (Zn), metallic Ag (Ag), SnO_2 (Sn), FeAsS (As), Sb_2S_3 (Sb), metallic Te (Te), metallic Co (Co), GeS_2 (Ge), and Bi_2S_3 (Bi).

Microthermometric measurements on doubly polished thin sections (<1 mm thick) were carried out using the Chaixmeca heating and freezing stage at the University of Mining and Geology "St. Ivan Rilski", Sofia, Bulgaria. It has a temperature range from −180 °C to +600 °C.

Sulfur was extracted from 10 pure pyrite separates. Sulfur isotope analysis was undertaken by Elemental Analysis – Isotope Ratio Mass Spectrometry (EA-IRMS) at the Iso-Analytical Limited, Crewe, Cheshire, United Kingdom. Prior to analysis the samples were crushed and ground to a powder using a pestle and mortar. Small amounts (0.25 mg) of samples were weighed into tin capsules (8 × 5 mm) along with 4 mg of vanadium pentoxide catalyst to aid combustion. Tin capsules containing reference or sample material plus vanadium pentoxide catalyst were loaded into an automatic sampler. After that they were dropped into a furnace held at 1080 °C and combusted in the presence of oxygen. Tin capsules flash combust, raising the temperature in the region of the sample to ~1700 °C. The combusted gases are then swept in a helium stream over combustion catalysts (tungstic oxide/zirconium oxide) and through a reduction stage of high purity copper wires to produce SO_2, N_2, CO_2, and water. Water is removed using a Nafion™ membrane. Sulfur dioxide is resolved from N_2 and CO_2 on a packed GC column at a temperature of 32 °C. The resultant SO_2 peak enters the ion source of the IRMS where upon it is ionized and accelerated. Gas species of different mass are separated in a magnetic field then simultaneously measured on a Faraday cup universal collector array. Analysis was based on monitoring of *m/z* 48, 49 and 50 of SO^+ produced from SO_2 in the ion source. Both references and samples are converted to SO_2 and analyzed using this method. The analysis proceeds in a batch process by which a reference is analyzed followed by a number of samples and then another reference. The reference material used for sulfur isotope analysis was IA-R061 (barium sulfate, $\delta^{34}S_{V\text{-}CDT}$ = +20.33‰). IA-R061, IA-R025 (barium sulfate, $\delta^{34}S_{V\text{-}CDT}$ = +8.53‰) and IA-R026 (silver sulfide, $\delta^{34}S_{V\text{-}CDT}$ = +3.96‰) were used for calibration and correction of the ^{18}O contribution to the SO^+ ion beam. IA-R061, IA-R025 and IA-R026 standards are traceable to NBS-127 (barium sulfate, $\delta^{34}S_{CDT}$ = +20.3‰) and IAEA-S-1 (silver sulfide, $\delta^{34}S_{V\text{-}CDT}$ = −0.3‰). NBS-127 and IAEA-S-1 are inter-laboratory comparison standards distributed by the International Atomic Energy Agency (IAEA) with internationally accepted $\delta^{34}S$ values.

4. Hydrothermal alteration

The styles of alteration are propylitic, sericite, argillic, and advanced argillic. Alteration mineralogy is based on investigations using optical microscopy and XRD.

Propylitic alteration dominantly occurs in the outer parts of the Milin Kamak deposit.

The *chlorite-carbonate-epidote alteration* assemblage (Fig. 4A, B) is common while the *chlorite-carbonate-epidote-actinolite* is rare. Relicts of primary pyroxene and plagioclase phenocrysts can be often observed in the carbonate groundmass. Plagioclase phenocrysts are almost completely altered to carbonate (Fig. 4B). Pyroxene is replaced by chlorite (Fig. 4B). Later quartz-sericite-pyrite nests and carbonate veins are recognized. Pyrite is common and forms disseminations and fine veinlets.

Sericite or quartz-sericite-pyrite (QSP) alteration is structurally controlled and vein-related. The groundmass consists of fine-grained quartz, sericite, illite, phengite and rare calcite and dolomite with disseminated anhedral pre-ore pyrite (Fig. 4C, D). The original rock texture is poorly preserved and formed by plagioclase phenocrysts which are completely altered to sericite (Fig. 4D).

Argillic alteration zone is rare, fracture controlled and dominated mainly by clay minerals (Fig. 4E). XRD results indicate the presence of kaolinite, illite, sericite, quartz, pyrite, and rarely anatase, nacrite, calcite and dolomite. Smectite group minerals are not found.

Advanced argillic alteration zone is developed in the northern part of the deposit at the No. 8 ore zone. This alteration style hosts the copper mineralization. Quartz-kaolinite and quartz-kaolinite-alunite assemblages are well developed while vuggy quartz zone is scarce (Fig. 4F, G, H). Aluminium phosphate-sulfate (APS) minerals such as svanbergite, woodhouseite and rare florencite are documented by XRD.

5. Mineralogy

The most common textural types of ores are: 1) symmetrically and asymmetrically banded ore, formed from quartz-sulfide and carbonate-sulfide veinlets (Fig. 5A); occasionally stockworks are observed; 2) disseminated and nest-like texture, formed from the main sulfide minerals (Fig. 4F); 3) massive pyrite, sphalerite, galena ore (Fig. 5B); 4) carbonate-sulfide cemented breccia with altered host rock fragments (Fig. 5C); 5) crustiform banded ore; and 6) comb texture, composed from quartz or calcite (Fig. 5D).

On the basis of mineral assemblages, depositional sequence, crosscutting relationships, and textures, the vein mineralization can be referred to three ore stages: quartz-pyrite, quartz-polymetallic, and carbonate-gold. Fig. 6 shows the generalized depositional sequence of vein minerals.

Quartz-pyrite stage has simple mineral composition – quartz, euhedral to subhedral pyrite, trace pyrrhotite and hematite in the upper levels of the deposit.

Quartz-polymetallic stage is represented by major anhedral pyrite, galena, sphalerite; minor chalcopyrite, tennantite, bournonite, tellurides and electrum; and trace pyrrhotite, arsenopyrite, marcasite. The gangue minerals are quartz and carbonates.

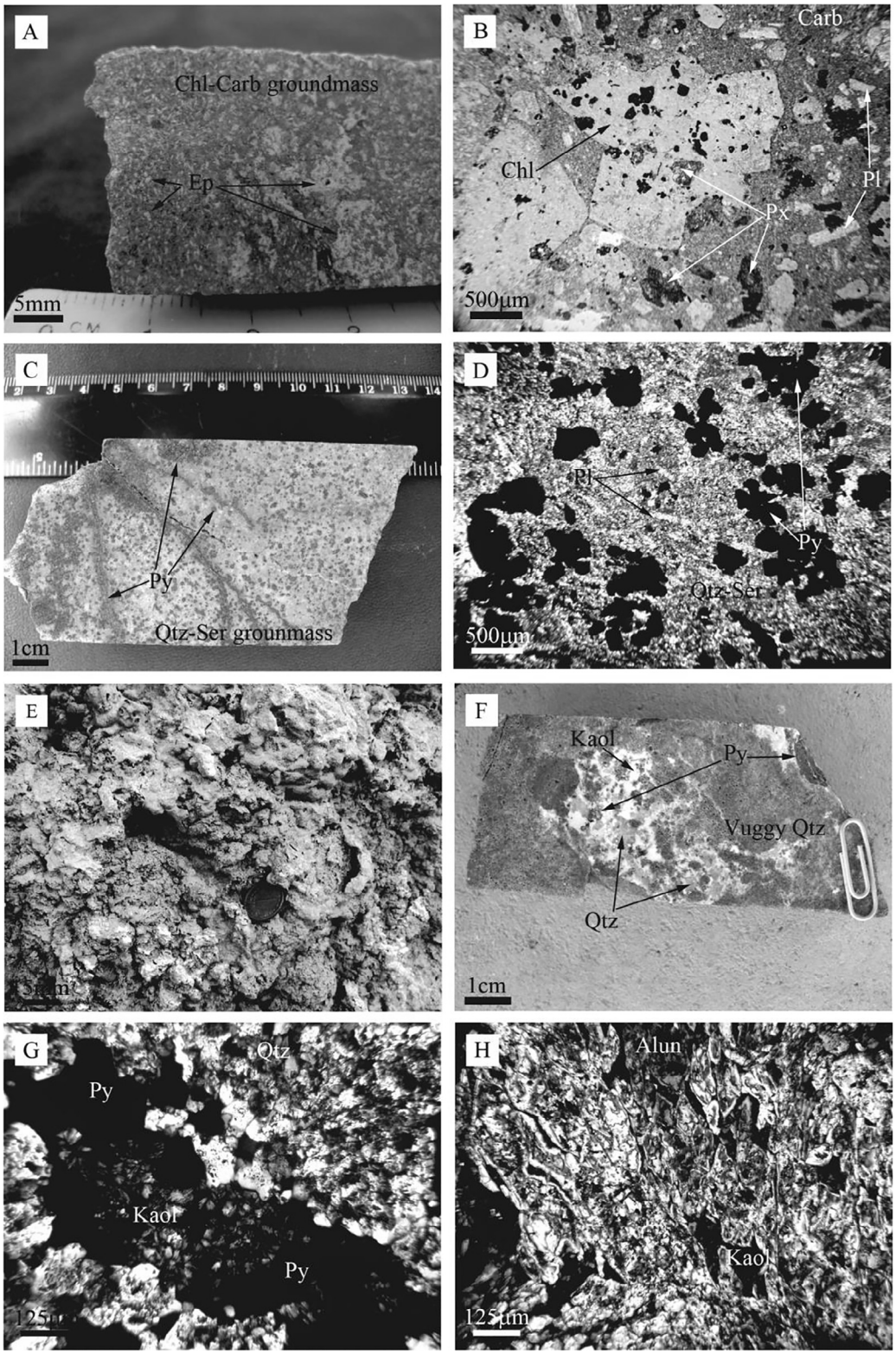

Fig. 4. Macroscopic textures and photomicrographs of alteration assemblages at the Milin Kamak: (A) Propylitic alteration (drill hole 10109, 34.1 m). The chlorite (Chl)-carbonate (Carb)-epidote (Ep) alteration assemblage is most common. (B) Photomicrograph of propylitic alteration. Relicts of primary pyroxene (Px) and plagioclase (Pl) phenocrysts can be often observed in the carbonate (Carb) groundmass. Plagioclase phenocrysts relicts are almost completely altered to carbonate. Pyroxene is replaced by chlorite. (C) Sericite alteration (drill hole 768, 122.2 m). The groundmass is represented by fine-grained quartz (Qtz) and sericite (Ser) with disseminated pyrite (Py) and pyrite veins. (D) Photomicrograph of the sericite alteration assemblages under crossed nicols. Plagioclase (Pl) phenocrysts are completely altered to sericite (Ser). The pyrite (Py) is anhedral. (E) Macroscopic view of the argillic alteration zone observed in the Bardoto Hill. The mineral assemblage is dominated mainly by clay minerals. (F) Advanced argillic alteration (drill hole 10105, 58 m). Vuggy quartz (Qtz) zone is rare. Main minerals in the alteration assemblage are kaolinite (Kaol) and quartz (Qtz). Pyrite (Py) is disseminated or infills cracks. (G) Photomicrograph of the quartz (Qtz)-kaolinite (Kaol) assemblage under crossed nicols. Kaolinite is observed as nests with pyrite (Py) grain rims in fine-grained quartz groundmass. (H) Photomicrograph of the quartz (Qtz)-kaolinite (Kaol)-alunite (Alun) assemblages under crossed nicols. The interstices between alunite crystals with rhombic forms are filled with kaolinite and quartz.

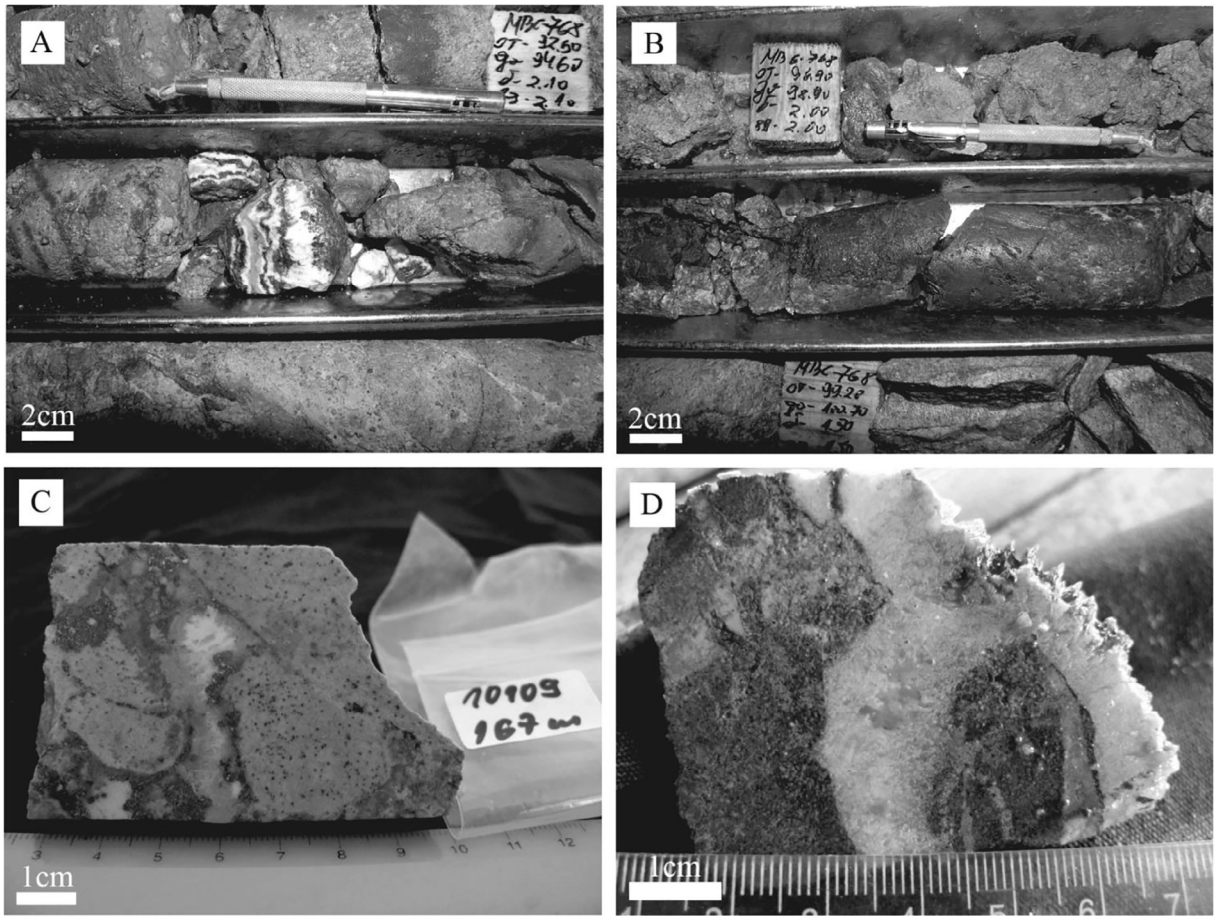

Fig. 5. Photographs of vein textures: (A) symmetrically banded ore, formed from carbonate-sulfide (mostly rhodochrosite and galena) veinlets (drill hole 768); (B) massive pyrite ore (drill hole 768); (C) carbonate-sulfide (rarely quartz) cemented breccia with altered host rock fragments (drill hole 10109); (D) comb calcite vein in altered host rock (drill hole 10109).

The last ore stage is *carbonate-gold*, defined by deposition of carbonate minerals and barite with native gold and stibnite.

The *supergene alteration* consists of sulfate and oxide-hydroxide minerals.

The *copper paragenesis* is observed only in samples from drill hole 10105 from No. 8 ore zone, NE part of the deposit. The mineral paragenesis of this ore zone is not included in the generalized paragenetic scheme because the obtained mineralogical data are not sufficient to relate the copper paragenesis with the others mineral stages. Nevertheless the paragenesis is important for the genetic interpretation of the deposit. The minerals are pyrite, chalcopyrite, chalcocite, covellite, and bornite. Alteration accompanying the copper mineralization is advanced argillic.

5.1. Ore mineralogy and mineral chemistry

5.1.1. Pyrite

Pyrite is the most common mineral and the only sulfide deposited in two ore stages. Pyrite I from the quartz-pyrite stage is euhedral to subhedral with cubic and octahedral forms. It occurs as single grains and fine- to medium-grained aggregates in quartz. Occasionally pyrite hosts pyrrhotite grains. Pyrite II usually forms subhedral to anhedral, rarely euhedral crystals and nests with size up to 2–3 cm. Very often pyrite is porous and marcasite occurs at the rims of the grains (Fig. 7A). Porous morphology, marcasite rims and the weak to distinct optical anisotropy of pyrite, suggest a secondary origin of the pyrite and its formation by inversion from marcasite (Murowchick, 1992). Pyrite II is enclosed in galena and sphalerite from the quartz-polymetallic stage or in the interstices of pyrite grains or in cavities of corroded pyrite (Fig. 7B).

5.1.2. Galena

Galena is the second-most abundant sulfide mineral in the quartz-polymetallic stage. It forms nests, fills fractures and pores mainly in quartz and occurs mainly as grains, inclusions and veinlets in pyrite and rarely in the other sulfides, also fills interstices of pyrite aggregates (Fig. 7B). Numerous blebs of coprecipitated electrum and tellurides (hessite, petzite and altaite) are observed in galena (Fig. 7E). Electrum infills microfractures and cleavage gaps (Fig. 7E). Electron microprobe analyses reveal the presence of Ag, As, Fe, Cd, and rarely Zn and Cu as trace elements (Table 1). These elements are inherent for the galena and probably are due to inclusions of sulfide minerals (Blackburn and Schwendeman, 1977).

5.1.3. Sphalerite

Sphalerite is deposited in the quartz-polymetallic stage. It occurs as nests, sometimes as veinlets among or together with the other sulfide minerals. In some samples sphalerite encloses pyrite or forms thin veinlets, crosscutting the pyrite aggregates, indicating that it formed later than pyrite. Commonly, tennantite and bournonite enclose and crosscut the sphalerite (Fig. 7C, D). Irregularly distributed small chalcopyrite inclusions with spherical or drop-like forms, known as “chalcopyrite disease” are observed in sphalerite (Fig. 7B, C). This phenomenon can be interpreted as a result of replacement due to interaction of sphalerite with solutions, coprecipitation of sphalerite and chalcopyrite, crystal growth by solid-

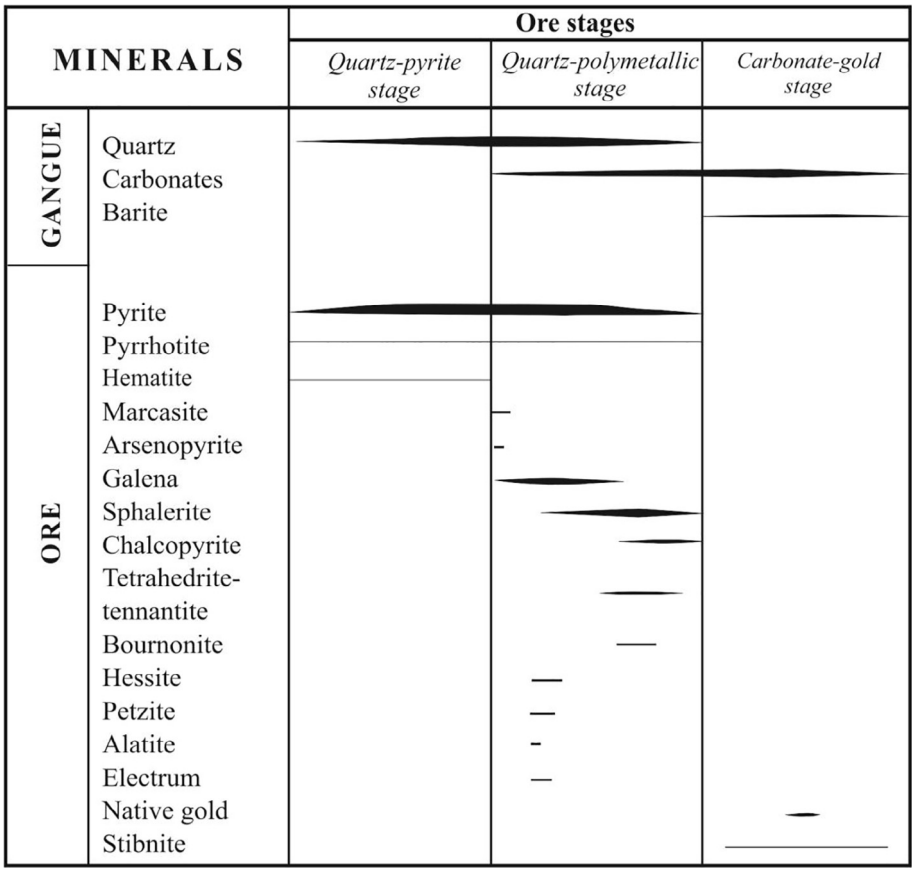

Fig. 6. Generalized depositional sequence of ore and gangue minerals at the Milin Kamak gold-silver deposit. Thick lines show major minerals, thin lines – minor minerals. Stages of mineralization are described in the text.

state diffusion and exsolution of CuS in Fe-bearing sphalerite. The main factors controlling these processes are the iron content of sphalerite, the volume relationships, temperature and the variations in sulfur fugacity (Wiggins and Craig, 1980; Bortnikov et al., 1991; Bonev and Radulova, 1994). Sphalerite from the Milin Kamak deposit is Fe-poor (0.16–0.91 wt.% or 0.22–1.27 mol%, only one analysis shows 8.16 wt.% or 11.42 mol%), so Fe contents are not determinant for the formation of chalcopyrite disease (Table 1).

The mole percent FeS in sphalerite coexisting with pyrite or pyrrhotite is continuously variable as a function of sulfidation state (Scott and Barnes, 1971; Czamanske, 1974). According to Einaudi et al. (2003) the mole percent FeS in sphalerite at intermediate sulfidation should range from 20 to 1%. The FeS contents in sphalerite from Milin Kamak deposit are similar to others intermediate sulfidation type epithermal deposits such as the Gandy and Abolhassani, Northern Iran (0.8–1.6 mol%) (Shamanian et al., 2003) and Sahinli and Tespih Dere, Western Turkey (0.6–1.4 mol%) (Yilmaz et al., 2010).

Sphalerite is an important carrier of a wide range of minor and trace elements. Cadmium is one of the most important trace element in sphalerite. Its contents normally vary in the range from 0.2 to 1.0 wt.% (Cook et al., 2009). Higher concentration are rare and are typical for some Mississippi Valley type deposits, such as Red Dog, Alaska (Kelley et al., 2004). Sphalerite is the main ore of Cd but abandoned mines and tailings dumps can represent a major environmental hazard (Schwartz, 2000; Murciego et al., 2010). At the Milin Kamak deposit Cd contents are low – within the 0.2–0.42 wt.% range (Table 1) and cadmium should not represent environmental risk. Gold contents vary from 0.66 to 0.70 wt.% (Table 1). Copper contents are low and probably this is due to "chalcopyrite disease".

5.1.4. Chalcopyrite

Chalcopyrite occurs as irregular grains, forms fine nests and veinlets among large pyrite aggregates and gangue minerals. Commonly chalcopyrite inclusions are typical in sphalerite as "chalcopyrite disease". In most samples tennantite encloses chalcopyrite but rarely the opposite relations are observed, indicating that tennantite predates or coprecipitate with chalcopyrite in close physicochemical conditions (Fig. 7C).

5.1.5. Tennantite

Tennantite occurs with the other sulfide minerals from the quartz-polymetallic stage. It is observed as inclusions in sphalerite and enclose pyrite and galena together with chalcopyrite. In some samples it associates with bournonite (Fig. 7D). Based on electron microprobe analyses and according to the "50-% rule" (Nickel, 1992) the members of the tennantite-tetrahedrite series are determined mostly as zincian tennantite. Gold (0.60 and 0.63 wt.%) and silver (1.25 and 0.8 wt.%) contents are documented in tennantite (Table 1).

5.1.6. Bournonite

Bournonite is rare and occurs as anhedral crystals and aggregates on the boundary between galena and sphalerite with chalcopyrite (Fig. 7D). It fills fractures in sphalerite indicating its later deposition in the quartz-polymetallic stage. EMPA indicate variations in its chemical composition. The Sb content ranges between 17.39 wt.% and 26.22 wt.%. In two of the samples, As contents were detected (3.83 and 6.51 wt.%) (Table 1). Higher As content tend to correlate negatively with lower Sb content, indicating a substitution between the two elements. According to Wu and Birnie (1977) As substitutes for Sb in bournonite to at least an

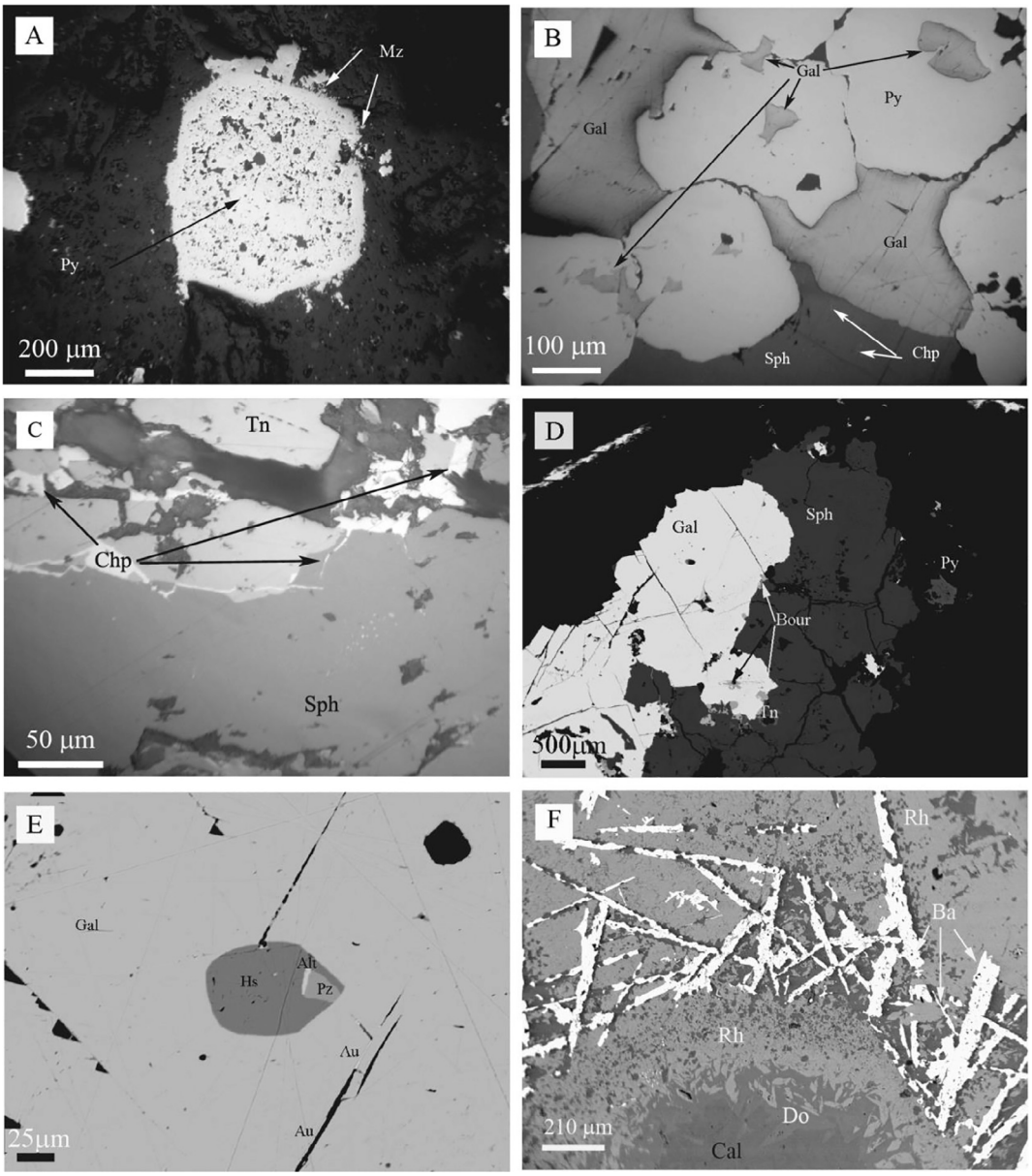

Fig. 7. Ore mineralogy (A, B, C – reflected plane-polarized light images; D, E, F – back-scattered electron images). (A) Euhedral pyrite (Py) with marcasite (Mz) rims (drill hole 768, 122.2 m). (B) Galena (Gal) infills the pyrite (Py) interstices and as inclusions in anhedral pyrite grains. Sphalerite (Sph) with "chalcopyrite (Chp) disease" encloses pyrite and galena (drill hole 10118, 89.6 m). (C) Chalcopyrite (Chp) on the crystal boundary between sphalerite (Sph) and tennantite (Tn) (drill hole 10114, 143 m). (D) Tennantite (Tn) and bournonite (Bour) deposited on the boundary between sphalerite (Sph) and galena (Gal) (drill hole 10109, 92.5 m). (E) Bleb of hessite (Hs), petzite (Pz) and altaite (Alt) in galena (Gal). Electrum (Au) from the quartz-polymetallic stage infills the cleavage gaps and cracks in galena in close spatial relation with telluride minerals (drill hole 10116, 115.9 m). (F) The upper part of a cavity with zonal deposition of rhodochrosite (Rh), dolomite (Do) and calcite (Cal). Barite (Ba) crystals are in rhodochrosite groundmass and are with multi-layered rim of rhodochrosite (drill hole 768).

As/(As + Sb) value (atomic) = 0.54. The authors assume a complete solid solution between bournonite and seligmannite. In bournonite from the Milin Kamak deposit the values As/(As + Sb) = 0.21 at.% (for 3.83 wt.% As) and As/(As + Sb) = 0.38 at.% (6.51 wt.% As) imply an As-bearing member of the bournonite-seligmannite series.

5.1.7. Telluride minerals

Hessite, petzite, and altaite are found for the first time at the Milin Kamak deposit. They occur as blebs up to 75 μm only in galena at depths of 115.9 m in drill hole 10116. The blebs are dominated by hessite and electrum (Fig. 8A). In rare cases altaite occurs instead of electrum (Fig. 7E). Hessite is the most common and always associates with petzite. Petzite is rare and enclose electrum or altaite in the blebs.

Electron microprobe analyses of telluride minerals show chemical composition close to stoichiometry. Au content in hessite reaches 0.92 wt.% and in altaite – 4.74 wt.% Ag (Table 1).

5.1.8. Gold

In the quartz-polymetallic stage electrum is deposited and in carbonate-gold stage – native gold.

Electrum occurs at depths of 115.9 m and together with hessite and petzite composite blebs in galena (Fig. 7E; 8A). It is deposited also in the fractures and in the cleavage gaps in galena but always in close spatial relation with telluride minerals (Fig. 7E). Therefore hessite and petzite are indicators for the presence of electrum in the deposit. The morphology of electrum grains varies according to the shape of the fracture or cavity they infill. Most often it occurs

Table 1
Representative compositions of minerals from the Milin Kamak gold-silver deposit.

Minerals	wt.%	S	Fe	Cu	Zn	As	Ag	Cd	Sb	Te	Au	Pb	Total	Representative formulae
Pyrite (n = 96)	Average	53.54	46.14	0.02	0.03	0.11	bdl	bdl	bdl	bdl	0.42	bdl	100.25	$Fe_{1.00}S_{2.01}$
	St. dev.	0.90	0.44	0.08	0.11	0.31	bdl	bdl	0.03	bdl	0.35	bdl		$(Fe_{1.00}As_{0.01})_{1.01}S_{2.00}$ $(Fe_{0.92}As_{0.09}Au_{0.01})_{1.02}S_{1.99}$
Galena (n = 9)	Average	14.84	1.69	0.02	bdl	1.28	0.05	0.98	bdl	bdl	bdl	81.82	100.69	$(Pb_{0.83}Fe_{0.11}As_{0.06}Cd_{0.02})_{1.02}S_{0.99}$
	St. dev.	0.73	1.80	0.07	bdl	0.75	0.16	0.15	bdl	bdl	bdl	3.11		$(Pb_{0.91}Cd_{0.02})_{0.93}S_{1.03}$
Sphalerite (n = 7)	Average	33.29	1.65	0.06	64.49	bdl	bdl	0.26	bdl	bdl	0.29	bdl	100.04	$Zn_{0.97}S_{1.02}$
	St. dev.	1.19	2.88	0.16	3.45	bdl	bdl	0.18	bdl	bdl	0.36	bdl		$(Zn_{0.99}Fe_{0.02}Cu_{0.01})_{1.02}S_{0.99}$ $(Zn_{1.00}Fe_{0.01})_{1.01}S_{0.99}$
Chalcopyrite (n = 1)		34.49	30.67	34.6	bdl	bdl	bdl	bdl	bdl	bdl	0.57	bdl	100.33	$(Cu_{1.00}Au_{0.01})_{1.01}Fe_{1.01}S_{1.98}$
Tennantite (n = 2)	Average	28.06	2.42	39.97	6.72	10.13	1.03	bdl	11.73	bdl	0.62	bdl	100.66	$(Cu_{9.91}Zn_{1.56}Fe_{0.35}Ag_{0.18}Au_{0.05})_{12.05}$ $(As_{2.24}Sb_{1.53})_{3.77}S_{13.2}$
	St. dev.	0.95	1.63	1.11	0.19	1.05	0.32	bdl	0.47	bdl	0.02	bdl		$(Cu_{9.34}Zn_{1.59}Fe_{0.97}Ag_{0.11}Au_{0.05})_{12.06}$ $(As_{1.90}Sb_{1.42})_{3.32}S_{13.58}$
Bournonite (n = 3)	Average	21.75	bdl	14.55	0.49	3.45	0.12	0.50	22.23	bdl	bdl	38.06	101.15	$(Pb_{0.76}Zn_{0.04}Cd_{0.02})_{0.82}Cu_{1.11}$ $(Sb_{0.83}As_{0.23})_{1.06}S_{3.01}$
	St. dev.	0.39	bdl	1.26	0.45	3.27	0.20	0.10	4.48	bdl	bdl	1.83		$(Pb_{0.86}Cd_{0.02})_{0.88}Cu_{0.97}Sb_{0.97}S_{3.11}$ $(Pb_{0.85}Ag_{0.01}Zn_{0.06}Cd_{0.02})_{0.94}Cu_{1.00}$ $(Sb_{0.64}As_{0.39})_{1.03}S_{3.00}$
Hessite (n = 2)	Average	0.20	bdl	bdl	bdl	bdl	61.71	bdl	bdl	33.96	0.46	bdl	96.32	$(Ag_{2.00}Au_{0.02})_{2.02}(Te_{0.92}S_{0.04})_{0.96}$
	St. dev.	0.28	bdl	bdl	bdl	bdl	1.40	bdl	bdl	1.41	0.65	bdl		$Ag_{1.99}Te_{0.94}$
Petzite (n = 2)	Average	bdl	bdl	bdl	bdl	bdl	40.73	bdl	bdl	30.19	22.21	4.09	97.20	$Ag_{3.09}Au_{0.93}Pb_{0.14}Te_{1.92}$
	St. dev.	bdl	bdl	bdl	bdl	bdl	1.12	bdl	bdl	1.04	0.35	0.98		$Ag_{3.14}Au_{0.93}Pb_{0.14}Te_{1.98}$
Altaite (n = 1)		bdl	bdl	bdl	bdl	bdl	4.74	0.52	bdl	35.91	bdl	57.60	98.77	$(Pb_{0.91}Ag_{0.14})_{1.05}Cd_{0.02}\ Te_{0.93}$
Electrum (n = 2)	Average.	bdl	bdl	0.12	bdl	bdl	20.87	bdl	bdl	bdl	73.25	6.66	100.89	$(Au_{0.69}Ag_{0.36}Pb_{0.05})_{1.1}$
	St. dev.	bdl	bdl	0.16	bdl	bdl	0.23	bdl	bdl	bdl	0.91	0.22		$(Au_{0.68}Ag_{0.35}Pb_{0.06}Cu_{0.01})_{1.1}$
Native gold (n = 2)	Average	bdl	0.33	0.76	bdl	bdl	7.02	0.37	bdl	bdl	79.20	5.94	93.60	$(Au_{0.83}Ag_{0.13}Pb_{0.06}Cu_{0.05}Fe_{0.02}Cd_{0.01})_{1.1}$
	St. dev	bdl	0.11	0.76	bdl	bdl	1.08	0.52	bdl	bdl	7.36	0.42		$(Au_{0.96}Ag_{0.16}Pb_{0.07}Cu_{0.01}Fe_{0.01})_{1.21}$
Stibnite (n = 3)	Average	28.17	0.04	0.11	bdl	0.37	bdl	bdl	70.03	bdl	0.61	bdl	99.32	$(Sb_{1.97}Cu_{0.02}Au_{0.01})_{2.00}S_{2.97}$
	St. dev.	0.35	0.07	0.18	bdl	0.64	bdl	bdl	0.27	bdl	0.10	bdl		$(Sb_{1.95}Au_{0.01})_{1.96}S_{2.99}$ $(Sb_{1.95}As_{0.05}Au_{0.01})_{2.01}S_{3.00}$

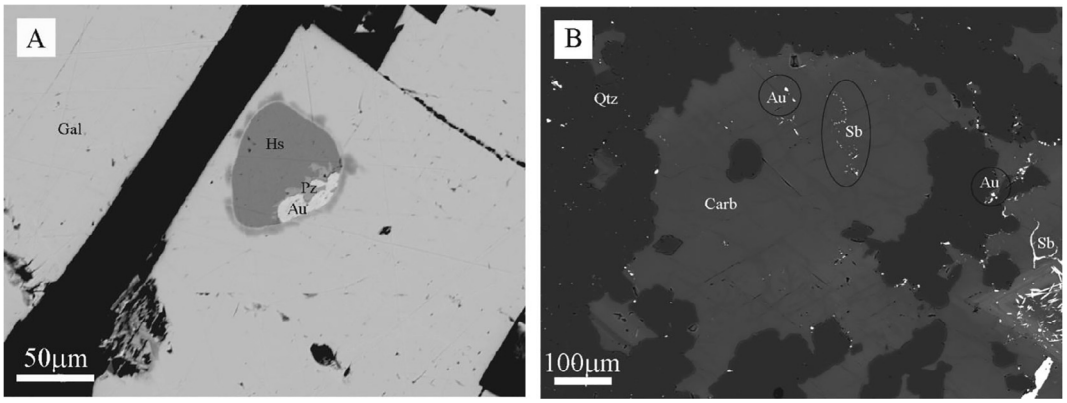

Fig. 8. Back-scattered electron images of gold. (A) Electrum from the quartz-polymetallic stage. Bleb of electrum (Au), hessite (Hs) and petzite (Pz) in galena (Gal) (drill hole 10116, 115.9 m). (B) Native gold from the carbonate-gold stage. Native gold (Au) grains and stibnite (Sb) in carbonate (Carb) and on the phase boundary with quartz (Qtz) (drill hole 10109, 92.5 m).

as irregular, elongated, rarely as oval and drop-like grains. In the blebs electrum is up to 40–50 μm but generally hard to be distinguished (3–5 μm). The colour is pale yellow. EMPA indicate that composition corresponds to electrum with 20.70–21.03 wt.% Ag and fineness 724–729 (Table 1). Cu is documented in one sample (0.23 wt.%). Pb ranges from 6.50 to 6.81 wt.% and the high contents are probably result from the host galena.

Native gold occurs at depths of 92.5 m in carbonates with stibnite and barite. It is observed mostly as free grains with equant and oval forms up to 7 μm in carbonates, and very often on the phase

boundary between carbonates and quartz (Fig. 8B). The grains are gold yellow with high fineness (838–854). EMPA reveal Ag (6.25–7.78 wt.%), Pb (5.64–6.23 wt.%), Fe (0.25–0.41 wt.%), and Cd (0.73 wt.%) (Table 1).

Electron microprobe analyses also show traces of gold in pyrite (0.47–1.13 wt.%), sphalerite (0.66–0.70 wt.%), tennantite (0.60 and 0.63 wt.%), hessite (0.92 wt.%), and stibnite (0.50–0.69 wt.%) (Table 1).

5.1.9. Stibnite

Stibnite is deposited in the carbonate-gold stage. It mainly occurs as unevenly distributed prismatic to needle-like crystals and forms nest among the carbonates (Fig. 8B). It rarely forms veinlets up to 1 cm. Stibnite is deposited mostly on the boundary between carbonates and quartz. EMPA reveal Au content from 0.50 to 0.69 wt.% (Table 1).

5.2. Gangue mineralogy and mineral chemistry

The most common gangue minerals are quartz, carbonates and barite.

5.2.1. Quartz

Quartz I is deposited in the quartz-pyrite stage. Massive quartz aggregates host and corrode pyrite I. Quartz II from the quartz-polymetallic stage is fine- to coarse-grained and infills fractures and cavities and rarely forms comb texture. Quartz II is commonly colourless, transparent, but rarely clear. In some samples grey to milky quartz can be observed. Trace chalcedony occurs sporadically in association with quartz.

5.2.2. Carbonate minerals

The carbonate minerals are deposited mainly in the carbonate-gold stage, whereas in the quartz-polymetallic stage they are rare. They are medium- to coarse-grained, rarely occur as euhedral crystals with scalenohedral habit. Based on electron microprobe analyses the members of the carbonate group from the carbonate-gold stage were determined as calcite, dolomite and rhodochrosite. Calcite is the most common carbonate mineral. It infills cavities together with dolomite and rhodochrosite. A distinctive zonal deposition of carbonates can be observed in cavities. The order of deposition from periphery to the center of the cavities is: rhodochrosite → dolomite → calcite (Fig. 7F).

5.2.3. Barite

Barite forms crystal laths up to 2 mm in length, rarely up to 0.5 cm in cavities with coarse-grained carbonates. Barite crystals often have multi-layered envelopes of rhodochrosite (Fig. 7F). Sr contents up to 3.42 wt.% define the barite as Sr-rich member of the barite-celestine series (Hanor, 2000).

5.3. Supergene minerals

Supergene alteration has affected the sulfides. The main supergene minerals are copiapite, epsomite, jarosite, iron and manganese oxide-hydroxides. The depth of weathering is related to the structure and level of the ground-water table and is about 2–5 m below surface.

5.4. Copper-bearing paragenesis

The copper paragenesis consists of pyrite, chalcopyrite, chalcocite, bornite, and covellite. Pyrite and chalcopyrite are primary, whereas chalcocite, bornite and covellite are supergene. Pyrite is deposited in two generations. Pyrite I occurs as porous and fractured euhedral to subhedral crystals. Pyrite II is anhedral and infills the interstices between pyrite I grains. It is also porous, fractured and brecciated. Chalcopyrite is rare and replaced by the supergene copper sulfides. Bornite occurs with chalcocite and together they form net-mesh-like microtextures in pyrite. Chalcocite is the main copper sulfide in the paragenesis. It encloses pyrite I and mainly infills fractures in pyrite II. Covellite replaces chalcocite rarely and occurs as free grains in the gangue groundmass. The gangue minerals are quartz, kaolinite and alunite.

6. Fluid inclusion petrography and microthermometry

The quartz samples were collected from the main No. 1 ore zone. Fluid inclusions are hosted by medium-grained quartz, which is the main gangue mineral in the deposit and associated with pyrite. It is commonly assumed that primary inclusions hosted by transparent gangue minerals which show a purely spatial association with ore minerals are representative of the ore-forming fluid (Wilkinson, 2001). Many of the collected samples did not contain inclusions of sufficient size and abundance to provide further study but still data was obtained from doubly polished sections (<1 mm thick) at depths of 64.8 m and 167 m (drill holes 1097 and 10109). Primary and secondary inclusions with no daughter minerals were identified. Only two-phase inclusions at room temperature were recognized. All of them are liquid-rich, containing 20–30 vol.% vapour (V) and 70–80 vol.% liquid (L) (Fig. 9).

Based on the occurrence in a single crystal without evidence of direction of growth or growth zonation, primary intracrystalline inclusions were defined. They occur as single inclusions which are large relative to that of the enclosing crystal and the size ranges from 5 to 20 μm. The shape of the inclusions is oval and equant. The secondary inclusions are randomly distributed in planar groups with irregular, elongated and rod shapes.

Using the criteria for primary origin of Roedder (1984) all results are believed to have been obtained from primary fluid inclusions. Microthermometric data are summarized in Table 2 and Fig. 10. The homogenization temperature (T_h) of the primary inclusions ranges from 238° to 345 °C (Fig. 10) and only three of the measurements are above 273 °C. Ice-melting temperatures (T_m) range from −2.2 to −4.1 °C and salinity – from 3.7 to 6.6 wt.% NaCl equiv. (Table 2). Salinity is calculated from ice-melting temperatures, using the revised equation of Bodnar (1993).

7. Sulfur isotope data

Sulfur isotope compositions were analyzed in 10 pure separates of pyrite from drill holes 10105, 10109 and 10114. The results are expressed using the delta per mil notation with respect to Canyon Diablo Troilite (V-CDT). The $\delta^{34}S$ values range from −0.49 to +2.44‰ (Fig. 11). The average calculated $\delta^{34}S$ values are 1.35‰ (Table 3). The total range of $\delta^{34}S$ values for pyrite are close to zero per mil which suggest a magmatic source for sulfur (Ohmoto and Rye, 1979; Seal, 2006).

8. Discussion

The Milin Kamak gold-silver deposit occurs within altered trachybasalt to andesitic trachybasalt volcanic and volcanoclastic rocks of Upper Cretaceous age. E-W-striking faults host the ore mineralization.

The geophysical IP anomaly, established by Trace Resources Ltd. suggests the presence of an intrusive body and probably a related porphyry mineralization (Crummy et al., 2001). In earlier publications fluid inclusions studies of quartz show homogenization temperature of about 400 °C which also imply for a porphyry body at depth (Stoykov et al., 2007; Moritz et al., 2007). The shallower

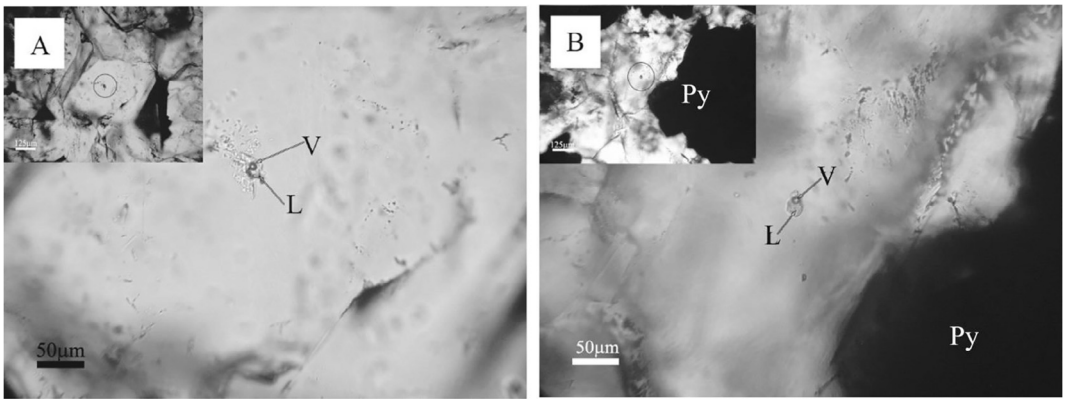

Fig. 9. Photomicrographs showing primary two-phase liquid-rich (L) fluid inclusions with vapor bubble (V) in quartz. (A) Primary fluid inclusion in quartz from drill hole 10109 at a depth of 167 m. On the left corner of the small microphotograph the quartz crystal with the location of the fluid inclusion can be observed. (B) Primary fluid inclusion in quartz in association with pyrite (Py) from drill hole 1097 at a depth of 64.8 m. On the left corner of the small microphotograph the quartz crystal with the location of the inclusion can be observed.

Table 2
Homogenization (T_h) and ice-melting (T_m) temperatures of primary fluid inclusions in quartz from the Milin Kamak gold-silver deposit.

Drill hole no./sample/depth	Number of the studied fluid inclusions	T_h °C (average)	Number of studied fluid inclusions	T_m °C (average)	wt.% NaCl equiv. (Bodnar, 1993)
10109/15/167 m	3	243.15 237.7 240	3	−2.2 −3.0 −3.2	3.7 5.0 5.3
10109/15-2/167 m	8	270.55 316.05 344.95 341.05 241.8 273.1 268.25 260.5	2	−3.5 −4.1	5.7 6.6
1097/64.80 m	2	243.2 260.75	5	−3.3 −2.7 −2.5 −3.4 −2.6	5.4 4.5 4.2 5.6 4.3

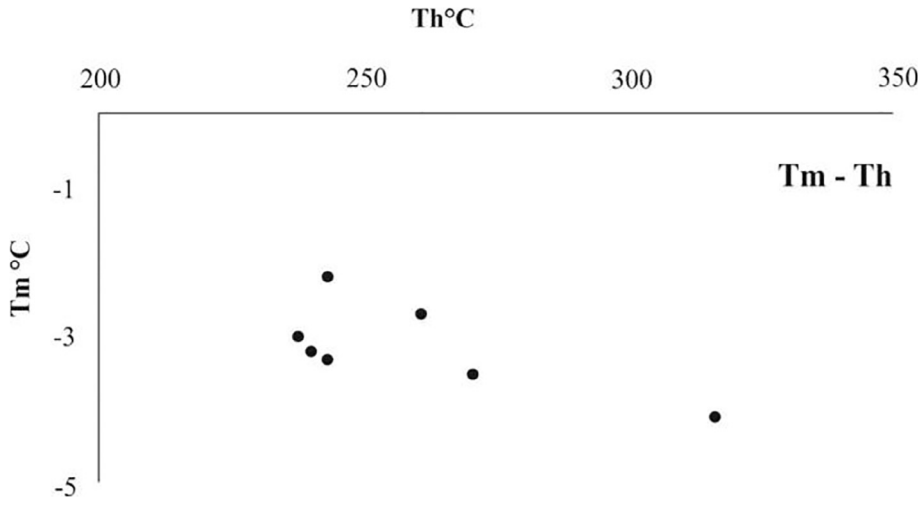

Fig. 10. Homogenization (T_h) vs. ice-melting (T_m) temperatures for primary fluid inclusions (T_h vs. T_m).

parts of the porphyry systems may host high and intermediate sulfidation epithermal base and precious metal mineralization (Corbett and Leach, 1998; Sillitoe, 1989; Hedenquist et al., 2000; Sillitoe and Hedenquist, 2003; Sillitoe, 2010).

High sulfidation epithermal Au, Ag, and/or Cu deposits are typically located in the lithocap environment above the porphyry body. They contain sulfide-rich assemblages of high sulfidation state, typically pyrite-enargite, pyrite-luzonite, pyrite-famatinite,

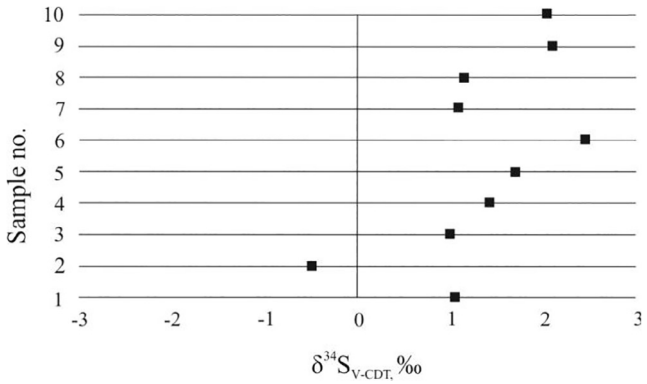

Fig. 11. Range of $\delta^{34}S$ values (‰) for pyrite samples from the Milin Kamak deposit.

Table 3
Stable S isotope values of the Milin Kamak gold-silver deposit.

Sample no.	Drill hole no./Ore zone no.	Sulfur content %	$\delta^{34}S_{V\text{-}CDT}$, ‰
1	10105/ 8	49.8	1.05
2		64.8	−0.49
3	10109/ 6; 1	53.0	0.98
4		48.2	1.42
5		48.9	1.69
6		60.0	2.44
7	10114/ 1	67.5	1.08
8		49.2	1.14
9		32.6	2.10
10		44.4	2.04
			Average 1.35

and pyrite-covellite, hosted by leached silicic rock with a halo of advanced argillic minerals (Hedenquist et al., 2000; Sillitoe and Hedenquist, 2003; Einaudi et al., 2003).

Most intermediate sulfidation epithermal Au and Ag deposits occur in calc-alkaline andesitic-dacitic arcs (Sillitoe and Hedenquist, 2003). A few intermediate sulfidation deposits, typically small ones, adjoin advanced argillic lithocaps, with or without associated high sulfidation deposits (Sillitoe, 1999). Some of them show a spatial association with porphyry systems (Sillitoe, 1989). This deposit type contains sulfide assemblage of intermediate sulphidation state, including FeS-poor sphalerite (from <1 to 10 mole percent FeS, locally up to 20 mole percent FeS), galena, pyrite, chalcopyrite, and tetrahedrite but lacking appreciable arsenopyrite and pyrrhotite. Silver is present as Ag sulfosalts, and in some cases a large variety of these minerals occur in trace amount. The main gangue minerals are Mn-bearing carbonates, rhodonite, and quartz (Hedenquist et al., 2000; Sillitoe and Hedenquist, 2003; Einaudi et al., 2003; Sillitoe, 2010).

The main characteristics of the high and intermediate sulfidation type epithermal precious metal deposits are shown on Table 4 in order to define the style of mineralization of the Milin Kamak deposit.

Advanced argillic alteration is observed only in the NE part of the Milin Kamak deposit, drill hole 10105, No. 8 ore zone. This style of alteration is an analogue of acid-sulfate alteration (Heald et al., 1987) and requires high oxidation and sulfidation state (Meyer and Hemley, 1967; Hemley et al., 1969). This ore zone consists of disseminated pyrite and copper sulfides – chalcocite, bornite, covellite with quartz, kaolinite, alunite and APS minerals. Alunite forms at temperatures of up to 500 °C and sulfate fluids with high

Table 4
Comparative characteristics of the main features of high and intermediate sulfidation type deposits (after Hayba et al., 1985; White and Hedenquist, 1995; Einaudi et al., 2003; Sillitoe and Hedenquist, 2003) and Milin Kamak deposit.

	High sulfidation	Intermediate sulfidation	Milin Kamak deposit	
			Ore zones 1, 2, 4, 6	Ore zone 8
Tectonic settings	Related to intrusive centers, rare calderas (Hayba et al., 1985)	Calc-alkaline andesitic-dacitic arc (Sillitoe and Hedenquist, 2003)^	High-K calc-alkaline arc, intrusive body and probably a related porphyry mineralization	
Host rocks	Mainly rhyodacite (Hayba et al., 1985) Andesite to rhyodacite (Sillitoe and Hedenquist, 2003)	Andesite to rhyodacite (locally rhyolite) (Sillitoe and Hedenquist, 2003)	Potassium trachybasalts and shoshonites, andesitic trachybasalt	
Deposit style and ore textures	Structure-controlled Disseminated, replacement ore little variation of ore textures: massive, rare veints and breccias (White and Hedenquist, 1995)	Open-space veins Wide variety of textures: crustiform, banded, comb, breccia (Sillitoe and Hedenquist, 2003)	Structure-controlled **Open-space veins**, stockwork, wide variety of textures	**Disseminated,** replacement ore, massive textures
Key alteration minerals	Quartz-alunite/APS; Quartz-pyrophyllite/dickite (Sillitoe and Hedenquist, 2003)	Sericite, without adularia (Sillitoe and Hedenquist, 2003) Illite ± adularia (Einaudi et al., 2003)	**Sericite without** adularia	Quartz-kaolinitequartz-kaolinite-**alunite** (APS)
Key sulfide species	Enargite, luzonite, famatinite, covellite (Sillitoe and Hedenquist, 2003)	Sphalerite, galena, tetrahedrite-tennantite, chalcopyrite (Sillitoe and Hedenquist, 2003) FeS-poor sphalerite (Einaudi et al., 2003)	Galena, **FeS-poor** sphalerite tetrahedrite-tennantite, chalcopyrite	**Chalcocite, bornite, covellite**, chalcopyrite,
Au and Ag	Native gold, rarely electrum (White and Hedenquist, 1995)	Native gold, electrum, native silver (Sillitoe and Hedenquist, 2003)	**Native gold, electrum, "invisible" gold Ag** и **Ag-Au tellurides**	"Invisible" gold
Gangue minerals				
Silica	Massive silicification and vuggy quartz (Sillitoe and Hedenquist, 2003)	Vein-filling crustiform and comb quartz (Sillitoe and Hedenquist, 2003)	Vein-filling crustiform and comb quartz	"Vuggy" quartz
Carbonate	Absent (Sillitoe and Hedenquist, 2003)	Common with manganiferious varieties (Sillitoe and Hedenquist, 2003)	Calcite, dolomite, **rhodochrosite**	Absent
Other	Late barite (Sillitoe and Hedenquist, 2003)	Barite ± manganiferious silicates (Sillitoe and Hedenquist, 2003)	Barite	Absent
Metal signature				
Main metals	Au-Ag, Cu, As-Sb (Sillitoe and Hedenquist, 2003) Commonly Cu + Au-Ag (Hayba et al., 1985)	Au-Ag, Ag-Au, Ag-pollymetallic, pollymetalic-Ag-Au, Ag, Zn, Pb, Cu (Sillitoe and Hedenquist, 2003)	**Au-Ag**	**Cu**, Au
Minor metals	Zn, Pb, Bi, W, Mo, Sn, Hg (Sillitoe and Hedenquist, 2003)	As, Sb, Mo (Sillitoe and Hedenquist, 2003)	Pb, Zn, Cu, As, Sb, Mn	As?
Te and Se	Tellurides common ± selenides (Sillitoe and Hedenquist, 2003)	Tellurides common, sellenides uncommon (Sillitoe and Hedenquist, 2003)	**Tellurides-common**	Absent

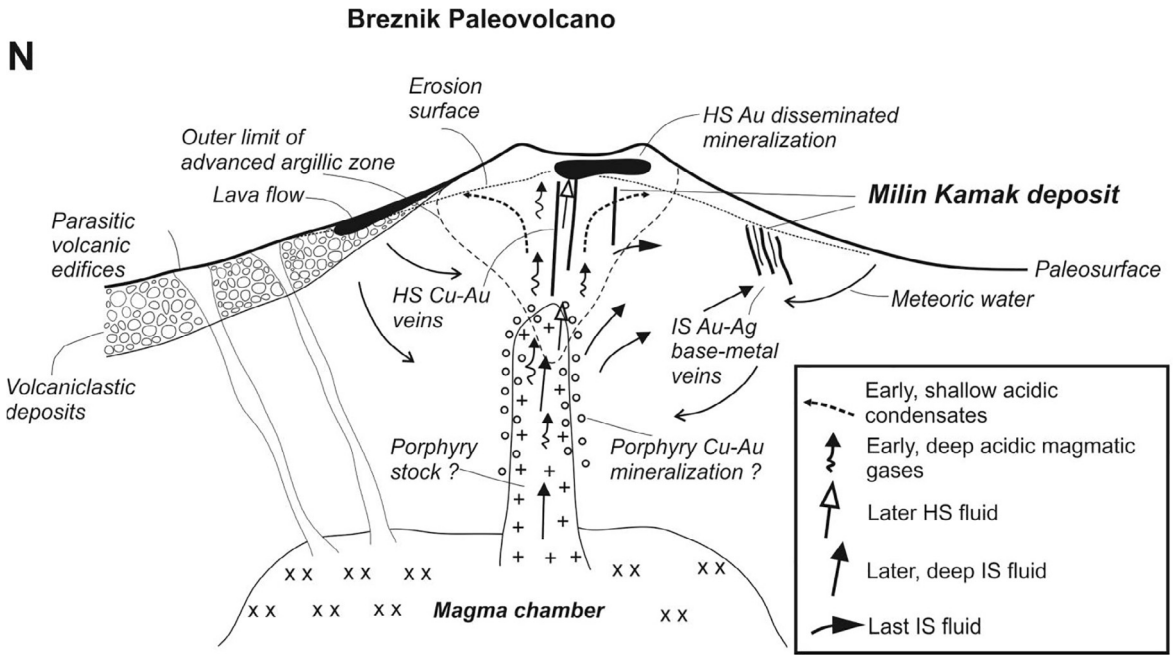

Fig. 12. Schematic section of Breznik paleovolcano showing relationships between high- and intermediate sulfidation type epithermal mineralization with the probable intrusive body (porphyry stock) and porphyry mineralization. On the norther slopes products of Breznik paleovolcano are situated (Velev et al., 2012). The probable migration and evolution of fluids are shown (after Sillitoe and Hedenquist (2003) with additions and modifications).

oxygen potential and low pH (0.8–5.3) (Hemley et al., 1969; Kashkai and Babaev, 1976). According to Ripp et al. (1998) APS minerals form in conditions of high activity of PO_4^{3-} ions, high oxygen potential and a pH interval from strong acid to neutral (3–8). The co-existence of these minerals suggests formation of the advanced argillic alteration zone in the Milin Kamak deposit in pH interval of 3–5. The presence of kaolinite in association with alunite and APS minerals indicates formation temperature of about 200 °C. These features point to the presence of high sulfidation type of mineralization which is around the center of Breznik paleovolcano and probably in a close genetic relationship with the intrusive body and the probable porphyry system which correspond with the model of Sillitoe and Hedenquist (2003) (Fig. 12) (Table 4).

On the southern slopes of Breznik paleovolcano relatively distant from the volcanic center No. 1, 2, 4 and 6 ore zones are situated (Fig. 12). A number of important features in these zones indicate the occurrence of intermediate sulfidation type mineralization. The epithermal veins associate with sericitic alteration without adularia. Ore mineralization exhibits a variety of textures – veins, veinlets, and stockworks; disseminated and nest-like texture; breccias; crustiform banded ore and comb texture. The ore minerals are dominated by pyrite, galena, FeS-poor sphalerite (0.22–1.27 mol% FeS), tennantite, chalcopyrite, electrum, and native gold. Tellurides are common. Gangue minerals are mainly quartz, calcite, dolomite, rhodochrosite, and barite (Table 4).

A similar transition between the high and intermediate sulfidation type mineralization, and the spatial association with a porphyry system is noted at many deposits including the Acupan and Antanamok intermediate sulfidation type deposits in Baguio district, Philippines which share a spatial and temporal relationship with the Kelly high sulfidation type deposit and the Ampucao porphyry (Sillitoe, 1989; Aoki et al., 1993; Cooke and McPhail, 2001; Cooke et al., 2011) and several deposits (Valea Morii and Rosia Poeni) in the South Apuseni Mountains of Romania (Ivascanu et al., 2002).

The homogenization temperature of primary inclusions in quartz ranges from 238° to 345 °C. The fluids are with low- to moderate salinity (from 3.7 to 6.6 wt.% NaCl equiv.). The total range of $\delta^{34}S$ for pyrite are close to zero per mil which point to a magmatic source for the sulfur (Ohmoto and Rye, 1979; Seal, 2006). The homogenization temperature, salinity and sulfur stable isotopes results suggest the impact of dominant meteoric and subordinate magmatic ore-forming fluids and confirm the epithermal environment (Einaudi et al., 2003; Pirajno, 2009).

9. Conclusions

The Milin Kamak gold-silver deposit is the first described epithermal deposit in the Western Srednogorie zone, Bulgaria. The deposit is located at the Breznik paleovolcano of Upper Cretaceous age between two big porphyry copper districts – Bor-Majdanpek to the west and Panagyurishte district to the east.

According to the geological setting, alteration style of the host rocks, main textures, mineral assemblages and composition of some minerals, depositional temperatures, salinities and sulfur stable isotopes Milin Kamak gold-silver deposit is an example for intermediate sulfidation type epithermal deposit which is in spatial and probably temporal association with high sulfidation mineralization and probable porphyry system.

Author's declaration

We wish to confirm that there are no known conflicts of interest associated with this publication and there has been no significant financial support for this work that could have influenced its outcome.

We confirm that the manuscript has been read and approved by all named authors and that there are no other persons who satisfied the criteria for authorship but are not listed. We further

confirm that the order of authors listed in the manuscript has been approved by all of us.

We confirm that we have given due consideration to the protection of intellectual property associated with this work and that there are no impediments to publication, including the timing of publication, with respect to intellectual property. In so doing we confirm that we have followed the regulations of our institutions concerning intellectual property.

Acknowledgments

This study was financially supported by Trace Resources Ltd and CEEPUS program for research stay at the University of Graz, Austria. The authors gratefully acknowledge Jürgen Neubauer (Institute of Earth Sciences, University of Graz) and Tsvetoslav Iliev (Geological Institute, Bulgarian Academy of Sciences) for their technical help with electron microprobe analyses and the scan images. We thank also Prof. Strashimir Strashimirov (University of Mining and Geology "St. Ivan Rilski") for the help during fluid inclusions studies.

References

Aoki, M., Comsti, E.C., Lazo, F.B., Matsuhisa, Y., 1993. Advanced argillic alteration and geochemistry of alunite in an evolving hydrothermal system at Baguio, northern Luzon, Philippines. Resour. Geol. 43, 155–164.

Arribas, J.A., 1995. Characteristics of high-sulfidation epithermal deposits, and their relation to magmatic fluid. In: Thompson, J.F.M. (Ed.), Magmas, fluids, and ore deposits: Mineralogical Association of Canada, Short Course 2, 419–454.

Bairaktarov, I., 1989. Upper Cretaceous metallogeny of Western Srednogorie and Plana Mountain. PhD thesis, Research Institute for Mineral Resources, Sofia, 197 pp. (in Bulgarian).

Belev, S., 1967. Petrographic and tectonic research of Breznik hollow. Rev. Bulgarian Geol. Soc. 28 (2), 139–151 (in Bulgarian).

Berza, T., Constantinescu, E., Vlad, S.N., 1998. Upper Cretaceous magmatic series and associated mineralization in the Carpathian – Balkan Orogen. Resour. Geol. 48, 291–306.

Blackburn, W.H., Schwendeman, J.F., 1977. Trace-element substitution in galena. Can. Mineral. 15, 365–373.

Bodnar, R.J., 1993. Revised equation and table for determining the freezing point depression of H_2O-NaCl solutions. Geochim. Cosmochim. Acta 57, 683–684.

Bogdanov, B., 1987. The Copper Deposits in Bulgaria. Technika Publ. House, Sofia. 388 pp. (in Bulgarian).

Bogdanov, K., Mišković, A., 2014. Porphyry-Epithermal Systems of the Panagyurishte ore district, Central Srednogorie, Bulgaria. MDRU Short Course 82, 54 pp.

Bonchev, E., 1988. Notes sur la tectonique alpine des Balkans. Bull. Soc. Géol. France 4 (2), 241–249.

Bonev, I.K., Radulova, A., 1994. Chalcopyrite and sphalerite "diseases": crystal growth by solid state diffusion. IMA 16th General Meeting, Pisa-1994, Italy. Abstracts, 50.

Bortnikov, N.S., Genkin, A.D., Dobrovolskaya, M.G., Muravitskaya, G.N., Filimonova, A.A., 1991. The nature of chalcopyrite inclusion in sphalerite: exsolution, coprecipitation or "disease"? Econ. Geol. 86, 1070–1082.

Chambefort, I., 2005. The Cu-Au Chelopech Deposit, Panagyurishte District, Bulgaria: Volcanic Setting, Hydrothermal Evolution, and Tectonic Overprint of a Late Cretaceous High-sulfidation Epithermal Deposit. PhD thesis, University of Geneva, Terre et Environnement 52, 173 pp.

Ciobanu, C.L., Cook, N.J., Stein, H., 2002. Regional settings and geochronology of the Late Cretaceous banatitic magmatic and metallogenic belt. Miner. Deposita 37, 541–567.

Cook, N.J., Ciobanu, C.L., Pring, A., Skinner, W., Shimizu, M., Danyushevsky, L., Saini-Eidukat, B., Melcher, F., 2009. Trace and minor elements in sphalerite: a LA-ICPMS study. Geochim. Cosmochim. Acta 73, 4761–4791.

Cooke, D.R., Simmons, S.F., 2000. Characteristics and genesis of epithermal gold deposits. Rev. Econ. Geol. 13, 221–244.

Cooke, D.R., McPhail, D.C., 2001. Epithermal Au-Ag-Te mineralization, Acupan, Baguio District, Philippines: numerical simulations of mineral deposition. Econ. Geol. 96, 109–131.

Cooke, D.R., Deyell, C.L., Waters, P.J., Gonzales, R.I., Zaw, K., 2011. Evidence for magmatic-hydrothermal fluids and ore-forming processes in epithermal and porphyry deposits of the Baguio District, Philippines. Econ. Geol. 106, 1399–1424.

Corbett, G.J., Leach, T.M., 1998. Southwest Pacific Rim gold-copper systems: structure, alteration and mineralization. Society of Economic Geologists Special Publication 6, 236 pp.

Crummy, J., Mutafchiev, I., Velinov, I., Petrunov, R., 2001. The Breznik epithermal Au occurrence, Western Srednegorie – Bulgaria: an "atypical"(?) low-sulphidation hydrothermal system. In: Piestrzynski, A. et al. (Eds), Mineral deposits at the beginning of the 21st century, Balkema, Lisse. Proceedings 6th biennial SGA meeting, Cracow, Poland, 723–726.

Czamanske, G.K., 1974. The FeS content of sphalerite along the chalcopyrite-pyrite-bornite sulfur fugacity buffer. Econ. Geol. 69, 1328–1334.

Dabovski, C., Harkovska, A., Kamenov, B., Mavroudchiev, B., Stanisheva-Vasileva, G., Yanev, Y., 1991. A geodynamic model of the Alpine magmatism in Bulgaria. Geol. Balcanica 21 (4), 3–15.

Dabovski, C., Kamenov, B., Sinnyovsky, D., Vasilev, E., Dimitrova, E., Bairaktarov, I., 2009. Upper Cretaceous geology. In: Zagorchev, I., Dabovski, C., Nikolov, T. (Eds.), Mesozoic Geology of Bulgaria. Marin Drinov Academic Publishing House, Sofia, pp. 305–611.

Einaudi, M.T., Hedenquist, J.W., Inan, E.E., 2003. Sulfidation state of fluids in active and extinct hydrothermal systems: transitions from porphyry to epithermal environments. In: Simmons, S.F., Graham, I.J. (Eds.), Volcanic, Geothermal and Ore-forming Fluids: Rulers and Witnesses of Processes Within the Earth: Society of Economic Geologists Special Publication 10, 285–313.

Evans, A.M., 1993. Ore Geology and Industrial Minerals: An Introduction. Blackwell Publ., Oxford, p. 389.

Ferdov, S., Kunov, A., 2002. The occurrence Zlatousha, Sofia district – data for adularia-sericite epithermal type. Rev. Bulgarian Geol. Soc. 63, 131–137 (in Bulgarian with English abstract).

Hanor, J.S., 2000. Barite-celestine geochemistry and environments of formation. Rev. Mineral. Geochem. 40, 193–275.

Hayba, D.O., Bethke, P.M., Heald, P., Foley, N.K., 1985. The geological, mineralogical, and geochemical characteristics of volcanic-hosted epithermal precious metal deposits. In: Geology and geochemistry of Epithermal Systems. Economic Geology 2, 129–168.

Heald, P., Foley, N.K., Hayba, D.O., 1987. Comparative anatomy of volcanic-hosted epithermal deposits: acid-sulfate and adularia-sericite types. Econ. Geol. 82, 1–26.

Hedenquist, J.W., Arribas, A., Gonzalez-Urien, E., 2000. Exploration for epithermal gold deposits. In: Hagemann, S.G., Brown P.E. (Eds.), Gold in 2000: Reviews in Economic Geology 13, 245–277.

Heinrich, C.A., Neubauer, F., 2002. Cu – Au – Pb – Zn – Ag metallogeny of the Alpine – Balkan – Carpathian – Dinaride geodynamic province. Miner. Deposita 37, 533–540.

Hemley, J.J., Hostetler, P.B., Gude, A.J., Mountjoy, W.T., 1969. Some stability relations of alunite. Econ. Geol. 64, 599–612.

Ivanov, Z., 1998. Tectonics of Bulgaria. Habilitation Thesis, Sofia University, 675 pp. (in Bulgarian, unpublished).

Ivascanu, P.M., Rosu, E., Udubasa, G., 2002. Geodynamic control of magma emplacement and ore deposit formation: Case study of South Apuseni Mts. Neogene calc-alkaline magmatic belt, Romania. In: GEODE study centre on geodynamics and ore deposit evolution, near Grenoble, France, 2002, Working Group discussion paper, 3.

Janković, S., 1977. The copper deposits and geotectonic setting of Tethyan Eurasian metallogenic belt. Miner. Deposita 12, 37–47.

Kamenov, B., Nedialkov, R., Yanev, Y., Stoykov, S., 2003. Petrology of Late-Cretaceous ore-magmatic centers from Central Srednogorie, Bulgaria. In: Society of Economic Geologists. Guidebook series 36, 27–46.

Kashkai, M.A., Babaev, I.A., 1976. Comparative characterization of alunites and alunitized rocks in Bulgaria and Azerbaijan. Geochem. Mineral. Petrol. 5, 130–144 (in Russian with English abstract).

Kelley, K.D., Leach, D.L., Johnson, C.A., Clark, J.L., Fayek, M., Slack, J.F., Anderson, V.M., Ayuso, L.E., Ridley, W.I., 2004. Textural, compositional, and sulfur isotope variations of sulfide minerals in the Red Dog Zn–Pb–Ag deposits, Brooks Range, Alaska: implications for ore formation. Econ. Geol. 99, 1509–1532.

Kunov, A., Stamatova, V., Atanasova, R., Hristova, V., Stanchev, Ch., 2000. New data of wallrock alterations and ore mineralization from the Klisoura occurrence, Sofia district. Rev. Bulgarian Geol. Soc. 61, 143–150 (in Bulgarian with English abstract).

Lindgren, W., 1933. Mineral Deposits. McGraw-Hill, New York, p. 930.

Meyer, C., Hemley, J.J., 1967. Wallrock alteration. In: Barnes, H.L. (Ed.), Geochemistry of Hydrothermal Ore Deposits. Rinehart & Wilson Publ, New York, Holt, pp. 166–235.

Moritz, R., Kouzmanov, K., Petrunov, R., 2004. Late Cretaceous Cu-Au epithermal deposits of the Panagyurishte district, Srednogorie zone, Bulgaria. Schweiz. Mineral. Petrogr. Mitt. 84, 79–99.

Moritz, R., Petrunov, R., Stoykov, S., Todorov, J., Strashimirov, S., 2007. The Breznik gold prospect, late Cretaceous Srednegorie belt, Bulgaria: evidence for an epithermal system telescoping a porphyry environment. Proceedings of the Ninth Biennial SGA Meeting, Dublin 2007, 193-196.

Murciego, A.M., Ayuso, E.Á., Sánchez, A.G., Pascual, E.P., 2010. The occurrence of Cd and Tl in the sphalerite from El Losar del Barco Mine (Ávila, Spain): a potential environmental hazard. Macla 13, 163–164.

Murowchick, J.B., 1992. Marcasite inversion and the petrographic determination of pyrite ancestry. Econ. Geol. 87, 1141–1152.

Nachev, I., Ganeva, N., Milanova, Y., 1981. Upper Cretaceous sedimentology in Western Srednogorie. Paleontol. Stratigr. Lithol. 14, 29–64 (in Bulgarian).

Nakov, R., Kunov, A., Hikov, A., Velinova, N., 2010. The metasomatic rocks from Gurgulyatski Kamak area, Western Srednogorie. Specific features and ore prospective. In: Proceedings of National Conference "Geosciences 2010", 09–10 Dec. 2010, Sofia, Abstracts, 46–47. (in Bulgarian with English abstract).

Nakov, R., Kunov, A., Hikov, A., Velinova, N., 2016. The metasomatic rocks from Gurgulyatski Kamak area, Western Srednogorie. Specific features and ore

prospective. Review of the Bulgarian Geological Society 77, 5–18. (in Bulgarian with English abstract) (in press).
Neubauer, F., Heinrich, C., 2003. Late Cretaceous and Tertiary geodynamics and ore deposit evolution of the Alpine – Balkan – Carpathian – Dinaride orogeny. In: Eliopoulos, D.G. et al. (Eds.), Mineral Exploration and Sustainable Development. Millpress, Rotterdam, pp. 1133–1136.
Nickel, E.H., 1992. Solid solutions in mineral nomenclature. Can. Mineral. 30, 231–234.
Ohmoto, H., Rye, R.O., 1979. Isotopes of sulfur and carbon. In: Barnes, H.L. (Ed.), Geochemistry of Hydrothermal Ore Deposits. John Wiley and Sons, New York, pp. 509–567.
Pirajno, F., 2009. Hydrothermal Processes and Mineral Systems. Springer, Berlin, p. 1250.
Popov, P., Berza. T., Grubic, A., 2000. Upper Cretaceous Apuseni-Banat-Timok-Srednogorie (ABTS) Magmatic and Metallogenic Belt in the Carpathian-Balkan Orogen. ABCD-GEODE 2000 Workshop, Borovets, Bulgaria, Abstracts, 69-70.
Popov, P., Berza, T., Grubic, A., Dimitru, I., 2002. Late Cretaceous Apuseni-Banat-Timok-Srednogorie (ABTS) Magmatic and Metallogenic Belt in the Carpathian-Balkan Orogen. Geol. Balcanica 32, 145–163.
Popov, P., Strashimirov, S., Popov, K., Kanzirski, M., Bogdanov, K., Raditchev, R., Dimovski, S., Stoykov, S., 2012. Geology and Metallogeny of the Panagyurishte ore region. UMG Publ. House, Sofia. 227 pp. (in Bulgarian).
Ripp, G.S., Kanakin, S.V., Shcherbakova, M.N., 1998. Phosphate mineralization in metamorphosed high-alumina rocks of Ichetuyskoe ore occurrence (south-west Transbaikali). Proc. Russian Mineral. Soc. 127, 98–108 (in Russian with English abstract).
Roedder, E., 1984. Fluid inclusions. Mineralogical Society of America. Reviews in Mineralogy 12, 644 pp.
Schwartz, M.O., 2000. Cadmium in zinc deposits: economic geology of a polluting element. Int. Geol. Rev. 42, 445–469.
Scott, S.D., Barnes, H.L., 1971. Sphalerite geothermometry and geobarometry. Econ. Geol. 66, 653–669.
Seal, R.R., 2006. Sulfur isotope geochemistry of sulfide minerals. Rev. Mineral. Geochem. 61, 633–677.
Shamanian, G.H., Hedenquist, J.W., Hattori, K.H., Hassanzadeh, J., 2003. Epithermal precious- and base-metal mineralization in the Eocene arc of Torud-Chah Shirin mountain range: Gandy and Abolhassani districts, Semnan, northern Iran. In: Eliopoulos, D.G. et al. (Eds.), Mineral Exploration and Sustainable Development. Millpress, Rotterdam, pp. 519–522.
Sillitoe, R.H., 1989. Gold deposits in western Pacific island arcs: the magmatic connection. Econ. Geol. Monograph 6, 274–291.
Sillitoe, R.H., 1999. Styles of high-sulphidation gold, silver and copper mineralization in the porphyry and epithermal environments. In: Weber, G. (Ed.), Pacrim '99 Congress, Bali, Indonesia, 1999, Proceedings: Parkville, Australasian Institute of Mining and Metallurgy, 29–44.
Sillitoe, R.H., Hedenquist, J.W., 2003. Linkages between Volcanotectonic Settings, Ore-Fluid Compositions, and Epithermal Precious Metal deposits. In: Simmons, S.F., Graham, I.J. (Eds.), Volcanic, geothermal and ore-forming fluids: Rulers and witnesses of processes within the Earth: Society of Economic Geologists Special Publication 10, 315–343.
Sillitoe, R.H., 2010. Porphyry copper systems. Econ. Geol. 105, 3–41.
Stanisheva-Vassileva, G., 1980. The Upper Cretaceous magmatism in Srednogorie Zone, Bulgaria: a classification attempt and some implications. Geol. Balcanica 10 (2), 15–36.
Stoykov, S., Strashimirov, S., Moritz, R., Dimitrov, D., Todorov, J., 2007. Mineral composition of the Breznik-Bardoto Au epithermal ore occurrence (Preliminary data). Ann. of the University of Mining and Geology 50 (1), Geology and Geophysics, 117–122.
Strashimirov, S., Petrunov, R., Kanazirski, M., 2002. Porphyry-copper mineralization in the Central Srednogorie zone, Bulgaria. Miner. Deposita 37, 587–598.
Velev, S., Nedialkov, R., Peytcheva, I., von Quadt, A., 2012. Geological and petrological characteristics of the volcanic centers from the Upper volcanogenic-sedimentary unit from the Western Srednogorie, Bulgaria. Geol. Macedonica 3, 7–12.
von Quadt, A., Moritz, R., Peytcheva, I., Heinrich, C., 2005. Geochronology and geodynamics of Late Cretaceous magmatism and Cu-Au mineralization in the Panagyurishte region of the Apuseni-Banat-Timok-Srednogorie belt. Ore Geol. Rev. 27, 95–126.
White, N.C., Hedenquist, J.W., 1995. Epithermal gold deposits: styles, characteristics and exploration. SEG Newsl. 23, 1–13.
Wiggins, L.B., Craig, J.R., 1980. Reconnaissance of the Cu-Fe-Zn-S system: sphalerite phase relations. Econ. Geol. 75, 742–751.
Wilkinson, J.J., 2001. Fluid inclusions in hydrothermal ore deposits. Lithos 55, 229–270.
Wu, I.J., Birnie, R.W., 1977. The bournonite-seligmannite solid solution. Am. Mineral. 62, 1097–1100.
Yilmaz, H., Oyman, T., Sonmez, F.N., Arehart, G.B., Billor, Z., 2010. Intermediate sulfidation epithermal gold-base metal deposits in Tertiary subaerial volcanic rocks, Sahinli/Tespih Dere (Lapseki/Western Turkey). Ore Geol. Rev. 37, 236–258.